Alterations in Autophagy and Senescence in the Pathologically Aged Uraemic Heart

William White

Queen Mary University of London

Submitted in partial fulfilment of the requirements of the

Degree of Doctor of Philosophy

2016

Statement of originality

I, William White, confirm that the research included within this thesis is my own work or that where it has been carried out in collaboration with, or supported by others, that this is duly acknowledged below and my contribution indicated. Previously published material is also acknowledged below.

I attest that I have exercised reasonable care to ensure that the work is original, and does not to the best of my knowledge break any UK law, infringe any third party's copyright or other Intellectual Property Right, or contain any confidential material.

I accept that this the College has the right to use plagiarism detection software to check the electronic version of the thesis.

I confirm that this thesis has not been previously submitted for the award of a degree by this or any other university.

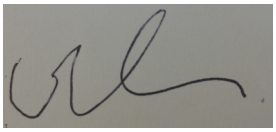

01/12/2016

Acknowledgements

I would like to thank my supervisor Professor Magdi Yaqoob for allowing me to undertake research in such a novel and interesting field, and for his time, teaching and example, both as an academic and clinician. I would like to thank Dr Steve Harwood for his practical support, and for his seemingly boundless patience and tolerance. I would like to thank Julius Kieswich for the time and effort he invested in generating uraemic animals for me. I would like to thank Dr Petros Andrikopoulos for instructing me in the finer points of immunoblotting, and Egle Solito for sourcing the GFP-LC3 mice, which were kindly supplied by Professor Noboru Mizushima at the University of Tokyo.

Abstract

There is much observational evidence to suggest that patients with chronic kidney disease are biologically 'older' than their unaffected peers. This is most obviously seen with cardiovascular disease: young patients on haemodialysis have a relative risk of cardiovascular mortality similar to that of people over 50 years their senior in the general population. Moreover, there are striking analogies between the effects of physiological ageing and uraemia on the structure and function of the heart and vasculature. Despite this, little work has been published looking at whether these similarities are reflected at a molecular and cellular level.

Two processes implicated in ageing are autophagy and senescence. There is much inferred evidence that these processes are affected by chronic kidney disease. The aim of this work was to investigate whether autophagy and senescence are indeed altered in the uraemic heart, whether these processes might be linked, and whether the findings of these enquiries might suggest their involvement in the pathogenesis of the prematurely aged cardiac phenotype.

An *in vitro* model of the uraemic myocardium was created using rat cardiac myoblast cells exposed to the uraemic toxin indoxyl sulphate, and *in vivo* models using adenine-diet and subtotal (5/6) nephrectomy rodents. Autophagy was assayed using immunoblotting, PCR array, immunohistochemistry and fluorescence microscopy, and senescence by immunoblotting and as part of an ageing-dedicated PCR array.

Though not achieving statistical significance, markers of autophagy activity appeared to be increased in rat cardiac myoblast cells exposed to indoxyl sulfate, and in cardiac tissue from adenine-diet rats. Interestingly markers of autophagy activity were significantly increased in hepatic tissue from subtotal nephrectomy rats. PCR of RNA purified from cardiac tissue from adenine-diet rats demonstrated an expression of ageing-related genes analogous to that in physiological ageing.

Though limited by numbers, these findings present evidence to suggest that autophagy may be upregulated as a protective mechanism in the progeroid uraemic heart, a situation possibly comparable to that in physiological ageing. Changes in cardiac autophagy and ageing in uraemia present new avenues for translational research into pathological ageing in chronic kidney disease.

Contents

List of Figures

List of Tables

Abbreviations

AMP	adenosine monophosphate
AMPK	5’adenosine monophosphate-activated protein kinase
APRCT	adenosine phosphoribosyltransferase
ATG	autophagy-related
ATM	ataxia telangiectasia mutated
ATP	adenosine triphosphate
BCA	bicinchoninic acid
BCL-2	b-cell lymphoma 2
BCL-XL	b-cell lymphoma extra large
CDK	cyclin-dependent kinase
CKD	chronic kidney disease
CMA	chaperone-mediated autophagy
CR	caloric restriction
DDR	DNA damage response
DMEM	Dulbecco’s Modified Eagle’s Medium
DMSO	dimethyl sulfoxide
EPC	endothelial progenitor cell
ER	endoplasmic reticulum

ESKD	end stage kidney disease
FCS	foetal calf serum
GAPDH	glyceraldehyde 3-phosphate dehydrogenase
GFP-LC3	green fluorescent protein-LC3
HCL	hydrochloride
HD	Huntington's disease
HSC	haematopoietic stem cell
IS	indoxyl sulphate
LAMP-2A	lysosomal-associated membrane protein 2A
LC3	microtubule-associated protein 1A/1B-light chain 3
LDL	low density lipoprotein
LVH	left ventricular hypertrophy
MEF	mouse embryonic fibroblast
MI	myocardial infarction
MOPS	3-(N-morpholino)propanesulfonic acid
MSC	mesenchymal stem cell
mTOR	mammalian target of rapamycin
NaCl	sodium chloride
PBS	phosphate buffered saline
PCR	polymerase chain reaction
PE	phosphatidylethanolamine

PI3	class III phosphatidylinositol-4,5-bisphosphate
PI3P	phosphatidylinositol 3-phosphate
p53	tumour suppressor protein 53
RB	retinoblastoma protein
ROS	reactive oxygen species
SASP	senescence-associated secretory phenotype
SA-β-GAL	senescence-associated beta-galactosidase
S100A8/A9	calgranulin A/B
SQSTM1/p62	sequestosome 1/p62
TASCC	TOR-autophagy spatial coupling compartment
TEM	transmission electron microscopy
TBS	tris-buffered saline
ULK1	unc-51-like autophagy activating kinase 1
VMP1	vacuole membrane protein 1

Chapter 1: Introduction

1.1 The accelerated ageing phenotype of chronic kidney disease (CKD)

Observation alone suggests that patients with advanced kidney disease are biologically older than their unaffected peers. As a group, patients with kidney disease have a morbidity and mortality profile similar to that of the geriatric population (Table 1), and the pathophysiology of the uraemic syndrome has interesting parallels with the ageing process. Based on these thoughts it has been posited that kidney failure results in accelerated, pathological ageing[1].

Ageing is a time-dependent, progressive loss of physiological integrity, leading to impaired function and increased vulnerability to death[2]. Dialysis dependent CKD patients of any age have an increased risk of mortality when compared to kidney transplant recipients and healthy controls of the same age[3], and are more susceptible to disease, particularly that of the cardiovascular system: a 25-34-year-old dialysis patient has a relative risk of cardiovascular mortality similar to that of a >75 year-old in the general population[4]. Indeed, there are striking analogies between the effects of ageing and uraemia on the structure and function of the heart and vasculature, with similar changes seen in pulse contour, pulse wave velocity, and impedance, and similar structural abnormalities with wall thickening, decreased elastin, and increased collagen content[5].

End stage kidney disease (ESKD) confers a greatly increased risk of infectious morbidity and mortality, whilst simultaneously being a chronic inflammatory state, a pattern of immune dysfunction also associated with ageing[6]. These abnormalities also seem to be reflected at a

cellular level, with preferential loss of cells belonging to the lymphoid cell lineage, and inflammation and expansion of pro-inflammatory immune cells[7].

There is a high prevalence of the frailty syndrome amongst CKD patients, a phenotype partly defined by weight loss, muscle weakness, and fatigue, which is associated with adverse outcomes in geriatric populations[8]. In the original study that developed this definition, 6.9% of participants ≥65 years-old (from a community-dwelling population) were classified as frail; in a more recent study of dialysis patients 44% of those under 40 years-old were found to be frail[9]. Cognitive impairment is also highly prevalent in the dialysis-dependent population and occurs in comparatively young patients[10].

Furthermore, the prognosis for CKD patients is still extremely poor and has not improved greatly despite many treatment advances: CKD patients receiving dialysis aged 50 and under are likely to live 30 years less than age-matched people without CKD[4]. Whilst survival rates have slightly improved they have not kept pace with the rises seen in the normal population without CKD, with the result that relative survival in age-specific patients with CKD actually decreased between 1977 and 2007[11]. There is thus an interest in identifying if CKD is inducing an ageing-like cellular and molecular dysfunction, and if so whether any novel potential therapy might be derived from an increased understanding of the pathways that are induced by both CKD and ageing. Whilst much has already been published on the intriguing similarities that appear to exist between the ageing process and CKD, comparatively little work has been undertaken looking at these cellular and molecular signs of aging in the context of the known evidence concerning uraemia-induced cellular and molecular pathways[12].

- Arteriosclerosis
- Valvular calcification
- Atherosclerosis
- Osteoporosis
- Sarcopaenia
- Oxidative stress
- Inflammation
- Poor wound healing
- Insulin resistance
- Infertility
- Hypogonadism
- Cognitive dysfunction
- Depression
- Frailty

Table 1: Characteristics of ageing seen in CKD[13]

1.2 The hallmarks of ageing

López-Ortín *et al* propose nine 'hallmarks of ageing', which contribute to the ageing process and determine the ageing phenotype. These are: genomic instability, epigenetic alterations, deregulated nutrient sensing, mitochondrial dysfunction, stem cell exhaustion, altered intercellular communication, loss of proteostasis (including decreased autophagy), telomere attrition and cellular senescence[2].

This thesis will focus primarily upon the possible involvement of autophagy and senescence in the pathologically aged uraemic phenotype. There is significant experimental evidence for the respective roles of these processes in normal organismal ageing, and for their complex interplay and interdependence. Moreover, whilst several observations have been made that hint at the involvement of autophagy and senescence in the uraemic syndrome, little has been published directly looking at this.

1.3 Senescence

Senescence may refer to the biological ageing of whole organisms (organismal senescence) and as such is often used interchangeably with the term 'ageing' itself. Cellular senescence, however, is defined as stable arrest of the cell cycle coupled to classic phenotypic changes[14]; use of the term 'senescence' will refer to this process from hereon in.

1.3.1 Mechanisms of senescence

Cellular senescence was originally described by Hayflick in serially passaged human fibroblasts, which undergo a certain number of divisions (the 'Hayflick limit') before entering a senescent phase[15]. This phenomenon was subsequently shown to be due to telomere shortening[16]. Replicative DNA polymerases are unable to fully replicate the terminal ends of linear DNA molecules, this function being restricted to a specialized DNA polymerase known as telomerase. Most mammalian somatic cells do not express telomerase, with the consequence that there is a progressive loss of protective telomere sequences from chromosome ends[2,17]. This eventually exposes an uncapped double-stranded chromosome end, triggering a permanent DNA damage response (DDR)[18]. In humans the DNA damage sensor ataxia telangiectasia mutated (ATM) is recruited to deprotected telomeres, leading to the induction of $p14^{ARF}$. This acts to stabilize the tumour suppressor protein 53 (p53), leading to the upregulation of the p53 transcriptional target p21. p21 inhibits cyclin-dependent kinase 2 (CDK2)-mediated inactivation of retinoblastoma protein (RB), with the result that the cell is prevented from entering into the S phase of the cell cycle[18,19,20,21]. A second barrier to proliferation, $p16^{Ink4a}$ prevents CDK4- and CDK6-mediated inactivation of RB to block cell cycle progression. This mechanism can act either alone or in combination with the p53-p21 pathway[18]. Both $p14^{ARF}$ and $p16^{Ink4a}$ are encoded for by the gene *CDKN2a*, thus activation of the *CDKN2a* locus promotes cellular senescence[22]. It is important to note that, contrary to historical understanding, senescence is not irreversible. For instance, activation of telomerase in senescent cells has the capacity to confer proliferative immortality[2].

In vitro senescent cells have several distinguishing characteristics, such as increased size[23], activity of the lysosomal hydrolase senescence-associated β-galactosidase (SA-β-GAL)[24], and the development of a senescence-associated secretory phenotype (SASP), which refers to their production of a variety of proinflammatory molecules, metalloproteases and growth factors[25,26].

1.3.2 Senescence and ageing

Senescent cells accumulate in aged organisms, though senescence *per se* does not cause ageing. Senescence prevents the propagation and causes the removal of damaged cells from tissues, and thus has an anti-oncogenic, protective effect. A failure to clear senescent cells and replace these with new ones may, however, lead to their accumulation, resulting in the loss of the tissue's regenerative capacity, and the development of an aged phenotype[2]. The role of $p16^{INK4a}$ and p53 in the induction of cell senescence suggests that their pro-ageing activity is the double effect of tumour suppression. One hypothesis proposes that, in healthy ageing, $p16^{INK4a}$ and p53 suppress the propagation of cellular damage and oncogenesis, but in conditions of pervasive damage this has a negative effect by simply accelerating ageing[2].

Shortening of telomeres during physiological ageing has been demonstrated in humans and mice[27]. Genetically modified mice with shortened or lengthened telomeres exhibit decreased or increased lifespans respectively[28,29], and the premature ageing of telomerase-deficient mice can be reversed with genetic reactivation of telomerase[30]. Physiological ageing in adult wild-type mice can be delayed by viral transduction of telomerase[31]. Telomerase deficiency in humans is associated with the premature development of diseases such as pulmonary

fibrosis, dyskeratosis congenita and aplastic anaemia, in all of which tissues lose their regenerative capacity[28]. There appears to be a strong correlation between shorter telomeres and mortality risk in humans, especially at younger ages[32].

CDKN2a, $p16^{INK4a}$ and $p14^{ARF}/p19^{ARF}$ (the murine equivalent) expression increases with age in all tissues studied in mice and humans[22]. Both $p16^{INK4a}$ and $p14^{ARF}/p19^{ARF}$ and are encoded by the *INK4a/ARF* locus, and a meta-analysis of genome-wide association studies identified the *INK4a/ARF* locus as that linked to the highest number of age-associated pathologies, including cardiovascular diseases and Alzheimer's disease[33]. Mutant mice with premature ageing produce increased levels of senescence markers, and this phenotype is improved by elimination of $p16^{INK4a}$ or p53[34]. However, mice with a mild increase in $p16^{INK4a}$ and p53 live longer[35], and the phenotype of progeroid mice is worsened by eliminating p53[36].

1.4 Autophagy

Proteostasis involves the maintenance of correctly folded proteins (by chaperones), and the appropriate breakdown of proteins by the proteasome or lysosome. Proteostasis is altered with ageing[37], and the subsequent increase in the expression of aberrant or aggregated proteins contributes to the genesis of age-related pathologies such as Alzheimer's disease[38].

The stress-induced production of cytosolic and organelle-specific chaperones, and the two primary protein degradation systems (the ubiquitin-proteasome and autophagy-lysosome systems), have all been determined to decline with ageing[2]. Experimentally increasing proteasome activity speeds up clearance of toxic proteins in cultured human cells[39], and

extends lifespan in nematodes[40]. This thesis, however, will focus on the autophagy-lysosome system.

The term 'autophagy', derived from the Greek meaning 'eating of self' was first used by Christian de Duve in the Journal of Cell Biology in 1967, when describing the degradation of mitochondria and other intra-cellular structures within lysosomes of rat liver perfused with glucagon[41]. Autophagy has traditionally been divided into macro-autophagy, micro-autophagy and chaperone-mediate autophagy (CMA)[42]. Micro-autophagy refers to the process by which structures in the cytoplasm are taken up directly by the lysosome[42]. In CMA proteins are carried into lysosomes in complexes with chaperone proteins that are recognized by lysosomal-associated membrane protein 2A (LAMP-2A) then degraded[43]. The term 'autophagy' typically refers to macro-autophagy (in which cytosolic cargo is delivered to the lysosome in autophagosomes)[42], and will do so henceforth in this thesis.

By removing and recycling excessive and aberrant organelles and proteins, autophagy both contributes to cellular homeostasis and protein quality control and functions as a source of energy for the cell[44].

Autophagy also has a complex crosstalk with cell death, and shares common machinery with these pathways. Whilst it often constitutes a stress response that avoids cell death (and suppresses apoptosis), under certain circumstances it may constitute an alternative cell death pathway. Autophagy and apoptosis may be triggered by common upstream signals resulting in combined autophagy and apoptosis. In other situations, cells may switch between two

responses in a mutually exclusive manner[45,].

1.4.1 Autophagy machinery

Much of our understanding of the molecular regulation and execution of autophagy derives from work done in yeast (*Saccharomyces cerevisiae*)[46], and it was for his contribution to this field that the 2016 Nobel Prize in Physiology or Medicine was awarded to Yoshinori Ohsumi. This thesis is restricted to coverage of what is known in mammals.

The process of autophagy is best explained in the context of nutrient starvation[47]. When energy in the form of adenosine triphosphate (ATP) is limited, 5' adenosine monophosphate-activated protein kinase (AMPK) becomes active, and this can engage autophagy. Deprivation from growth factors and/or amino acids leads to the inhibition of target of rapamycin complex 1 (TORC1, more commonly referred to as mammalian target of rapamycin, mTOR), which, when active, supresses autophagy. As a result of AMPK induction and/or mTOR inhibition, autophagy is initiated[48] (Figure 1).

The first event in autophagy is the forming of the isolation membrane or phagophore[49]. This engulfs portions of cytoplasm containing protein aggregates and organelles, enclosing them in a double-membraned vesicle named an autophagosome[50]. This autophagosome subsequently fuses with a lysosome to form an autolysosome, the contents of which are

broken down by lysosomal enzymes[42]. Amino acids and other products of degradation are exported back out to the cytoplasm via lysosomal permeases and transporters, for use in building macromolecules and metabolism[50].

A key component of the autophagosome is LC3-II, which is composed of a protein, microtubule-associated protein 1A/1B-light chain 3 (LC3), and a lipid, phosphatidylethanolamine (PE), and which is generated by a process involving E1, E2 and E3 ligases[48]. Its precursor molecule, LC3-I, is generated by the cleavage of LC3 by ATG4 (ATG is an abbreviation for 'autophagy-related'[51]) to produce LC3-I. LC3-1 is bound by the E1, ATG7, and transferred to the E2, ATG3. The E3 ligase complex is comprised of ATG16L and ATG12-5, the latter produced by another reaction in which ATG12 is bound by the E1, ATG7, transferred to a different E2, ATG10, and from there to ATG5. The process by which ATG12-5 is formed – and LC3-II is generated- being referred to as the elongation reaction and required for the formation of the autophagosome[48].

The origin of the isolation membrane/phagophore is not known for certain, though several sources have been suggested, including endoplasmic reticulum (ER) and the Golgi[52]. The initiation process depends upon the action of the Class III phosphatidylinositol-4,5-biphosphate 3-kinase (PI3 kinase) VPS34, which converts phosphatidylinositol to phosphatylinositol 3-phosphate (PI3P). The activity of VPS34 requires VPS15, a regulator, beclin 1, and other proteins, including ATG14L, that bind to beclin 1. The complex, termed the initiation complex, generates PI3P, which determines the site at which the double membrane

elongates by the E1-E2-E3 interaction described above[48].

During starvation-induced autophagy, the function of the beclin 1-VPS34 initiation complex is controlled by a preinitiation complex that includes a protein kinase, unc-51-like autophagy activating kinase 1 (ULK1), which activates the initiation complex to generate PI3P[53]. The preinitiation complex is activated by AMPK and inhibited by TORC1[54]. In the setting of glucose deprivation AMPK can also act directly on the beclin 1/VPS34 complex[55]. For starvation- and hypoxia-induced autophagy, it is also necessary to unleash negative regulators of the beclin 1-VPS34 initiation complex, such as B-cell lymphoma 2/B-cell lymphoma-extra large (Bcl-2/Bcl-xl)[54].

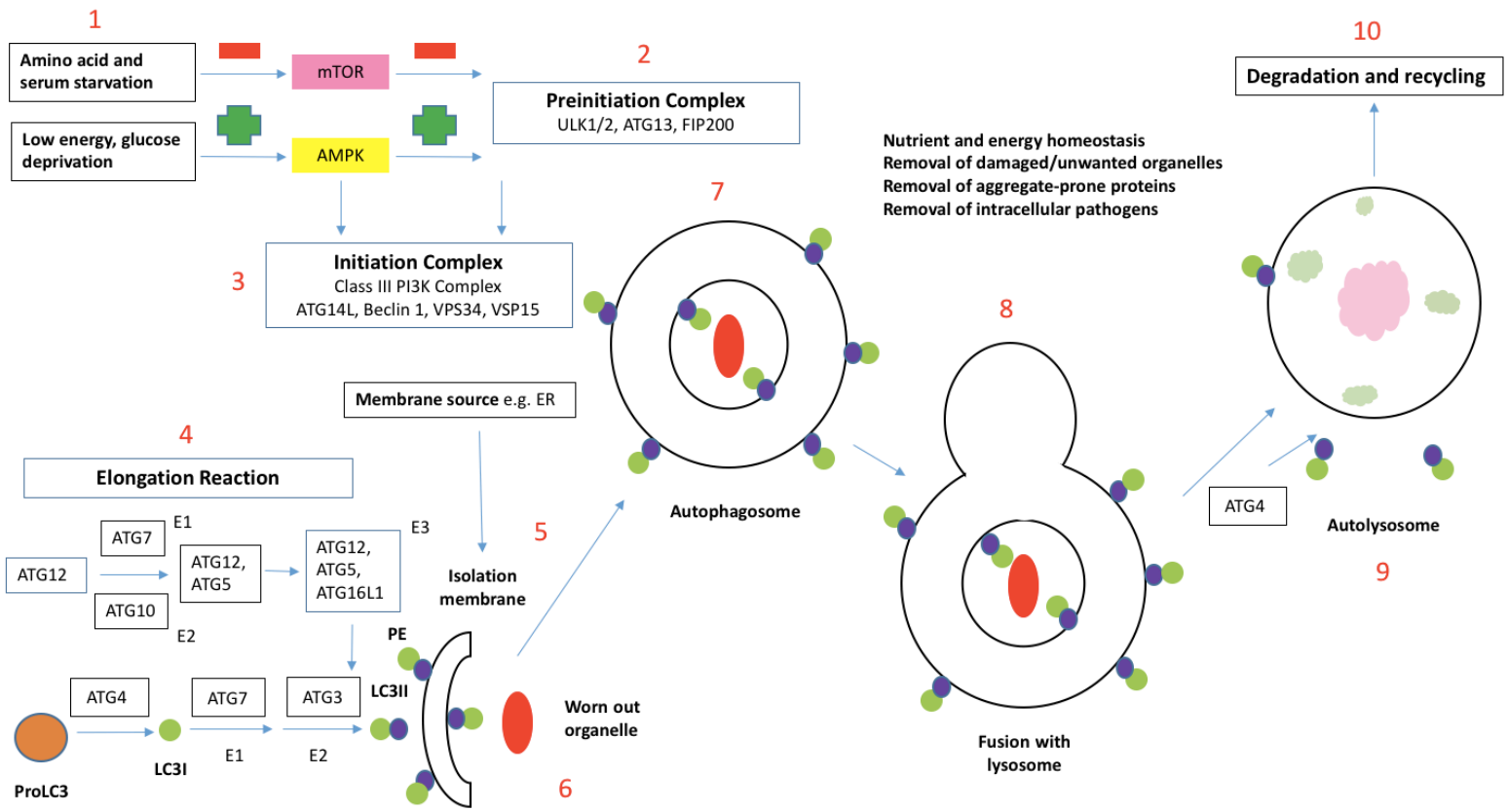

Figure 1: An overview of the autophagy pathway using the model of autophagy induction due to nutrient depravation: **1)** Amino acid and glucose deprivation inhibit and activate the mTOR and AMPK pathways respectively **2)** This results in stimulatory phosphorylation of ULK1/2 proteins in the 'preinitiation complex' **3)** The preinitiation complex activates the 'initiation complex' (also known as the Class III PI3K complex) via ULK-dependent phosphorylation. The initiation complex is also regulated by AMPK. The initiation complex generates PI3P at the site of formation of the isolation membrane (or phagophore), leading to the binding of PI3P binding proteins and the recruitment of proteins involved in the 'elongation reaction' to the isolation membrane **4)** In the elongation reaction the phosphatidylethanolamine-conjugated form of LC3 (LC3-II) is generated by the ATG4-dependent proteolytic cleavage of LC3, and the action of the E1 ligase, ATG7, the E2 ligase, ATG3, and the E3 ligase complex, ATG12/ATG5/ATG16L **5)** LC3-II associates with the isolation membrane, which **6)** expands to form a double-membrane structure, the autophagosome **7)** that surrounds cargo destined for degradation **8)** The autophagosome fuses with a lysosome to form a **9)** autolysosome, the contents of which are **10)** degraded and released into the cytoplasm for recycling. ATG4 cleaves LC3-II from the outside of the autolysosome to be returned to the cytosol, LC3-II on the inside being degraded.

1.4.2 Autophagy and ageing

Autophagy has been heavily implicated in the ageing process and the determination of life span[56]. It has been demonstrated that expression of Atg proteins and other proteins required for autophagy induction is reduced in aged tissues, and that autophagy diminishes with ageing[56]. For example, ATG5, ATG7, and beclin 1 have been shown to be downregulated in physiologically aged human brains[57]. Tissue-specific knockout of Atg genes precipitates age-associated stigmata in mice: these include the accumulation of ubiquitinylated protein-containing inclusion bodies, the appearance of the ageing pigment lipofuscin in lysosomes, disorganized mitochondria, and the oxidation then carbonylation, carboxymethylation or nitrosylation of proteins[56]. Zhang and Cuervo created an inducible hepatocyte-specific LAMP2a transgene to arrest the decline in LAMP2a levels in ageing mice. This restored defects in autophagy, and reduced the presence of oxidised proteins and polyubiquinated protein aggregates[58]. The observation by Melendez *et al.* that inhibition of the insulin-like growth factor pathway stimulates autophagy in *C.elegans* and that inhibition of autophagy by mutation of Atg genes prevents gain of longevity was the first to associate autophagy with longevity[59]. Caloric restriction (CR, reduced food intake without malnutrition) extends life span in all animals thus far tested, including non-human primates[60]. TOR inhibition, either pharmacologically (with rapamycin) or genetically, extends life span in yeast, *C.elegans*[61] and mice[62].

In postmitotic cells there is no cell division-mediated 'dilution' of intracellular debris, therefore autophagy makes an important contribution to protein homeostasis and organelle

turnover[56]. A number of experimental autophagy inducers, including rapamycin, can attenuate the accumulation of mutated Huntington protein and cell death in Huntington's disease (HD) models[63].

The mitochondrial theory of ageing suggests that ageing results from accumulating mitochondrial damage leading to progressive mitochondrial uncoupling with consequent bioenergetics insufficiency and increased production of reactive oxygen species (ROS)[64]. Autophagy inhibition results in deteriorated mitochondrial function in mice[65].

Autophagy may play a role in hormesis, the phenomenon whereby cells, organs, and organisms are able to resist typically lethal conditions after they have been exposed to sublethal damage[56]. One example of this is ischaemic preconditioning, wherein the exposure of tissues to short episodes of ischaemia subsequently protects them against infarction[56]. Autophagy is induced in ischaemic preconditioning[66] and is subsequently protective. Hormesis has been suggested as one of the many factors determining the rate of ageing[67].

Progressive numerical or functional decline of tissue stem cells may contribute to ageing[56]. Rapamycin increases life span[62] and restores self-renewal of haematopoietic stem cells (HSCs) in elderly mice[68]. Rapamycin can reverse stem cell loss in hair follicles as well as the resultant alopecia[69]. mTOR activation in HSCs of young mice mimics the phenotype of HSCs from elderly mice, causing a decrease in lymphopoiesis, an impaired capacity to replenish the haematopoietic system, as well as increased expression of the CDK inhibitors $p16^{Ink4a}$, $p19^{Arf}$ and p21[68].

Autophagy limits inflammatory reactions through several mechanisms. Autophagy in dying cells is required for clearing of apoptotic corpses, thus reducing inflammatory reactions[70]. Impaired autophagy results in the accumulation of p62/STQM1, which can activate the proinflammatory transcription factor NF-ΚB and the stress-responsive transcription factor NRF2, resulting in inflammation and tissue injury[71]. Autophagy also limits inflammation by eliminating dysfunctional mitochondria[72], and because pathological ageing is, commonly, accompanied by inflammation, the anti-inflammatory effects of autophagy may mediate health and lifespan benefits. Autophagy may contribute to improving the efficacy of pathogen recognition by immune effectors whilst reducing inflammatory reactions[56].

Interventions aimed at stimulating autophagy at a relatively mature age may have beneficial effects on ageing in mice[56]. Rapamycin treatment of middle aged mice (approximately 600 days) can extend their life span[62], and a 3-month period of CR can improve verbal memory in healthy aged humans[73]. Intermittent fasting can increase the life span of rodents as much as chronic CR without a concomitant major decrease in body mass[74].

1.5 Relationship between autophagy and senescence

The similarities between autophagy and senescence (both represent responses to stress that have potentially cytoprotective or cytotoxic functions) would suggest some form of co-existence, but if and how they work alongside one another remains to be fully elucidated[75]. Several investigators have provided indirect evidence for the simultaneous induction of autophagy and senescence (for example, an increase in numbers of autophagic vacuoles and senescence-associated β-galactosidase activity has been observed in ageing fibroblasts[76]), but these studies do not address whether autophagy and senescence are linked or interdependent.

Young *et al* demonstrated that pharmacologic and genetic approaches that interfere with autophagy delay the senescence response in fibroblasts. However, senescence in autophagy-compromised cells eventually achieved similar levels as in autophagy-competent cells, and senescence could not be reversed by autophagy abrogation[77]. This and studies with similar findings suggest that whilst autophagy can accelerate its onset, senescence induction in response to external or internal stressors does not obligatorily require prior autophagy.

In contrast, a number of other studies have been published supporting an inverse relationship between autophagy and senescence: i.e. inhibition of autophagy promotes the development of the senescent phenotype. Kang *et al* presented evidence that suppression of autophagy promotes senescence in fibroblasts, relating this to the increased generation of ROS by dysfunctional mitochondria when autophagy is compromised[78]. One hypothesis derived from this and other studies with similar findings is that senescence may act as a 'backup' response

in the event that autophagy fails to provide effective protection to injured cells and tissues.

Given the conflicting data, and the sensitivity to both processes to variations in experimental conditions between studies, there has hitherto been a lack of consensus as to if and how autophagy and senescence influence one another.

Very recent reports have suggested that autophagy may modulate several targets that act in opposition to regulate senescence. Thus, autophagy inhibition or promotion may result in different outcomes depending on the timing, duration, or type of its inhibition[79]. The transcription factor GATA4 is a key regulator of the SASP and senescence, and its stability is regulated by autophagy. Sequestosome 1/p62 (SQSTM1/p62, henceforth referred to as p62) mediates the degradation of GATA4 under normal conditions. However, once the cell experiences senescence-inducing stimuli, the interaction between GATA4 and p62 decreases, and GATA4 escapes from autophagic inhibition and accumulates. This accumulated GATA4 initiates a transcriptional circuit to activate NKKB/NF-κB and the SASP[80]. Kang *et al* demonstrated that transient inhibition of autophagy using an inducible small interfering RNA (siRNA) system stimulated senescence more than continuous inhibition, and that p62 depletion induces cellular senescence more than depletion of autophagy regulators ATG7 or ATG5. The authors suggest that selective autophagy suppresses cellular senescence through the breakdown of GATA4, whereas general autophagy supports senescence transition through the TOR-autophagy spatial coupling compartment (TASCC)[79]. Thus autophagy can act through either an anti- or prosenescence mechanism depending on its type of regulation.

Activation of TP53 (the gene encoding p53) initiates cell cycle arrest during cellular senescence. This activation is sustained even after cell cycle arrest is reinforced by activation of the CDKN2A/p16^{Ink4a} pathway, suggesting that the p53 pathway may have additional roles

beyond cell cycle arrest during senescence[18]. There is an ongoing dispute as to whether p53 activates, inhibits or variably regulates autophagy[81].

1.6 The effect of uraemia on autophagy and senescence

1.6.1 The effect of uraemia on autophagy

Autophagy has been found to have an important role in numerous physical processes aside from its one involved in ageing. It is up-regulated and has a protective function in the face of cellular stressors such as starvation[82] and ischaemia[83], and is increasingly being shown to play an important and protective role in a growing number of physiological and pathological processes, including the immune response[70], regulation of the inflammatory response[71], and the prevention of malignancy[84]. Whilst the involvement of autophagy in the genesis of kidney injury and disease has been the subject of investigation and review in the scientific literature[85], very little work has been done looking at the effect of kidney failure on autophagy in other tissues.

Uraemic individuals exhibit an increased susceptibility to numerous disease processes in which autophagy is thought to have a protective role, in addition to their accelerated ageing phenotype. As mentioned earlier, patients with CKD are known to have an increased rate of infectious and cardiovascular morbidity and mortality when compared to age- matched, healthy controls[4,6]. Using a rodent model of CKD and myocardial infarction, our group has previously demonstrated that uraemia reduces ischaemia tolerance and increases infarct size[86]. Observational studies of patients with CKD have demonstrated a high incidence of

malignant tumours[87], and CKD is known to be a chronic inflammatory state that predisposes to malnutrition, anaemia and atherogenesis in patients[88]. Given that autophagy is considered to have a protective function in these pathologies, it is possible that a perturbation of autophagy may contribute to their development, and that this may play a role in the tendency of uraemic patients to develop them: autophagy is dysfunctional in uraemia.

Very little has been published looking at the effects of established kidney disease on autophagy in tissues other than the kidney, and there is much scope for investigating this. Chen *et al*. assessed autophagy activation in circulating leucocytes taken from stage 5 CKD patients (uraemic and haemodialysed) and healthy controls, and concluded that autophagy is impaired in the former, that this is not reversed with haemodialysis[89]. Siedlecki *et al.* assessed the effect of rapamycin administration in a murine model of normotensive uraemic cardiomyopathy. Treatment of surgically induced renal injury mice with rapamycin blocked the development of cardiac hypertrophy and fibrosis when compared with vehicle-treated animals[90]. The experimenters suggest that this protective effect is mediated by the extracellular signal-regulated kinase and mammalian mTOR pathways, but do not speculate on the possible involvement of autophagy. They do, however, raise the interesting question of whether renal transplant recipients taking rapamycin as an immunosuppressant exhibit reversal of uraemia-induced cardiac changes beyond that associated with successful transplantation.

1.6.2 The effect of uraemia on senescence

Some studies have investigated the possible role of senescence and telomere attrition in uraemia. Jiminez *et al.* looked at markers of senescence in circulating immune cells in uraemic pre-dialysis, haemodialysis-dependent and transplanted patients. Abnormal telomere shortening was detected in immune cell subpopulations in pre-dialysis and haemodialysis patients who dialyzed with cellulosic membranes, but also in transplant recipients with near normal renal function[91]. It was thus unclear as to whether telomere shortening and immunosenescence was the result of uraemia *per se* or from chronic inflammation due to kidney disease, a bio- incompatible dialysis membrane, or in the case of the transplant patients due to major histocompatibility complex incompatibility and immunosuppressive therapy. Tsirpanlis *et al.* measured the activity of telomerase in peripheral blood mononuclear cells in haemodialysis-dependent patients and non-renal failure subjects. Telomerase activity was reduced in haemodialysis patients compared to healthy controls, and was lower in long-term than in short-term dialysis patients, again suggesting that it may be dialysis that causes senescence in these cells rather than kidney disease itself[92]. The Heart and Soul Study examined the association of kidney function with telomere length and telomere shortening in patients with stable coronary artery disease. This demonstrated that reduced kidney function is associated with shorter baseline telomere length and more rapid telomere shortening over 5 years, however, these associations were entirely explained by the age of the patients[93].

Several groups have looked at the role of senescence in the endothelial dysfunction associated with cardiovascular disease in uraemia. Adijiang *et al.* administered indoxyl

sulphate (IS, a uraemic toxin) to rats and examined their aorta for evidence of senescence. Treated animals showed significantly increased aortic calcification and wall thickness, and significantly increased expression of SA- β-gal, $p16^{Ink4a}$, p21, p53 and pRb in cells in the calcified area[94]. The same group went on to demonstrate that uraemic toxins stimulated senescence of cultured human aortic smooth muscle cells via an oxidative stress mechanism[95].

Carracedo *et al.* evaluated the effects of uraemic serum on endothelial progenitor cells (EPCs) obtained from healthy volunteers. EPCs were exposed to low-density lipoprotein (LDL) generated after incubation of native LDL (nLDL) with uraemic serum from patients with CKD stages 2-4. Compared with nLDL, the uraemic serum-treated LDL induced an increase in oxidative stress and senescence in EPCs, and a decrease in EPC proliferation and angiogenesis[96].

Klinkhammer *et al*. demonstrated that bone marrow mesenchymal stem cells (MSCs) isolated from uraemic rats (both surgically induced and adenine diet) showed signs of premature senescence, and failed to accelerate healing of glomerular lesions when injected into the left renal artery of rats with acute nephritis when compared to MSCs obtained from control rats[97]. Stem cell exhaustion and the resultant decline in tissue regenerative potential has been noted as one of the hallmarks of ageing[2].

1.7: Methodological challenges of assaying senescence and autophagy in uraemia

1.7.1 Assaying senescence

Identifying and isolating senescent cells *in vivo* is a major challenge. Senescent cells are thought to accumulate in aged tissues based on the detection of cells with high SA-β-GAL activity and expression of p53, p21, pRB and $p16^{Ink4a}$. However, the relative rarity of these cells, the nonspecificity of these markers and the lack of a good commercially available $p16^{Ink4a}$ antibody in mice have made studying senescence *in vivo* difficult[18]. *In vitro* senescent cells appear flattened and enlarged and similarly express p53, p21, pRB, $p16^{Ink4a}$ and SA-β-GAL as found *in vivo*.

1.7.2 Assaying autophagy

Autophagy is a notoriously elusive process to assay due to its complex spatiotemporal mechanics, and its responsiveness to multiple, subtle variables

'Autophagic flux' refers to the complete process of autophagy, which begins with the formation of the phagophore and ends with the destruction of the autolysosome[98]. It is important that multiple, complimentary assays are used to measure autophagic flux, and that the results of these are interpreted carefully, as a 'snapshot' measurement of one stage of the process cannot provide an accurate picture of overall activity, and may be misleading. For example, a common misconception is that increased numbers of autophagosomes in cells

corresponds to increased cellular activity. Given that the autophagosome is an intermediate structure, their number at any specific time point is a function of the balance between the rate of their generation and the rate of their conversion into autolysosomes and subsequent destruction: thus, autophagosome accumulation may represent either increased autophagy induction, or suppression of downstream steps[99].

In broad terms, in order to truly determine the state of autophagic flux it is necessary to follow either the decrease in an autophagy-degradable cargo or marker (whilst addressing the potential contribution of other degradative systems), or by arresting autophagic flux at given points and recording the accumulation of said cargo or marker[100].

1.7.2.1 Monitoring autophagic protein levels

LC3 is the most widely monitored autophagy-related protein, and exists in four isoforms that exhibit different tissue distributions, A, B, B2 and C, with LC3B being most commonly utilised[99]. LC3 is initially synthesized in an unprocessed form, proLC3, with a C-terminal extension that is removed by the protease ATG4 and becomes LC3-I. LC3-I is subsequently conjugated with PE by an enzymatic reaction to become LC3-II. Whereas LC3-I is localized in the cytoplasm, LC3-II associates with both the outer and inner membranes of autophagosomes. After fusion with the lysosome, ATG4 cleaves off LC3-II on the outer membrane, returning it to the cytosol, and lysosomal enzymes degrade LC3-II on the inner

membrane, resulting in low concentrations of LC3-II in the autolysosome. As the amount of LC3-II is closely correlated with the number of autophagosomes, detecting LC3 conversion (LC3-I to LC3-II) by immunoblot analysis is often used to monitor autophagy[101].

LC3-I and LC3-II are detected as two separate bands following gel electrophoresis and immunoblotting. ProLC3 is not detected under normal conditions as ATG4 processes it into LC3-I immediately after synthesis[102]. Although the molecular weight of LC3-II is greater than that of LC3-I due to the addition of PE, LC3-II migrates faster than LC3-I in gel, probably because of its extreme hydrophobicity[101]. LC3-I is usually detected on a gel at a molecular mass around 16 kD, and LC3-II at approximately 14 kD. The ratio between the two bands is often used as an indication of autophagic activity: an increase in the ratio of LC3-II to LC3-I signifying an increase in autophagosome formation. However, since LC3-II is itself degraded by the autophagic process, this may actually reflect a decrease in autolysosome formation and digestion.

LC3-II degradation can be inhibited by interrupting the process of autophagosome- lysosome fusion (for example using bafilomycin A1), or by inhibiting protein digestion in lysosomes (for example using chloroquine, which prevents lysosmal acidification)[103]. Differences in the amount of LC3-II between samples in the presence and absence of lysosomal inhibitors are a more accurate representation of autophagic flux. Furthermore, the sensitivity of detection of LC3-II by anti-LC3 antibodies is much higher than for that of LC3-I, particularly if antibodies generated against the N- terminal peptide are used. This suggests a conformational change is

produced at the N terminus after PE-conjugation, which allows better detection, presumably due to exposure of an antibody-reactive epitope[103]. Thus, comparing the amount of LC3-II among samples is likely to be more accurate than comparisons of LC3-I and LC3-II, or summation of LC3-I and LC3-II[103].

Another method for detecting autophagic flux is measuring p62 degradation. p62 binds to LC3 and it thus serves as a selective substrate of autophagy[104]. The level of p62 decreases during starvation (a potent autophagy-inducer) in wild-type mouse-embryonic fibroblasts (MEFs) but not in ATG5$^{-/-}$ MEFs, indicating that accumulation of p62 is an indicator of autophagy suppression[105]. However, the expression of p62 can be changed independent of autophagy[106], thus this information must be supported by data derived from other methods.

1.7.2.2 Monitoring transcriptional regulation

The induction of autophagy in certain scenarios is accompanied by an increase in the mRNA levels of certain autophagy genes, thus assessing these levels by polymerase chain reaction (PCR) may provide correlative data relating to the up-regulation of autophagy. For instance, transcriptional upregulation of vacuole membrane protein 1 (VMP1, a protein that is involved in autophagy regulation and that remains associated with the completed autophagosome) can be detected in mammalian cells subjected to rapamycin treatment or starvation, and in tissues undergoing disease-induced autophagy[107]. Complementary DNA (cDNA) arrays have

been developed to simultaneously monitor the transcriptional regulation of all (or a great number of) genes involved in, and related to, autophagy by PCR[108], thus permitting high throughput data collection. Several species- specific, validated microarrays are commercially available for this purpose[109].

Previous experimenters have demonstrated that changes in mRNA expression levels may be very subtle, and changes in protein levels may not accompany changes in the transcription of autophagy genes[102]. Therefore, changes in autophagy gene expression, whilst interesting, need to be accompanied by evidence of altered autophagic activity.

1.7.2.3 Monitoring numbers of autophagic structures

Numerous methods of 'directly visualising' autophagy have been utilised in published studies. Autophagy was first detected using transmission electron microscopy (TEM) in the 1950s[110]. At the ultrastructural level, an autophagosome is defined as a double- membraned structure containing undigested cytoplasmic contents (including organelles) that is yet to fuse with a lysosome[99]. However, interpreting TEM images requires a degree of expertise in order to distinguish autophagosomes from other cellular membranous structures.

Electron microscopy is being increasingly replaced by light microscopic and biochemical techniques. LC3 can be visualised by fluorescent microscopy either as a diffuse cytoplasmic pool (LC3-I), or as 'punctate' structures representing autophagosomes (LC3-II). An increase in autophagy activity is associated with an increase in the average number of punctae per cell[99]. LC3 can be labelled by using GFP-LC3 (green fluorescent protein-LC3) transfected mice[111].

Another approach, which eliminates the costs and difficulties inherent in transfection, and subsequently transfection efficiency validation, is to use a stain specific for autophagic vesicles.

Autophagy-related proteins can be detected in tissues using immunostaining[112]. A difficulty associated with this technique is the problem localizing LC3 to autophagic vacuoles, as opposed to the cytoplasm, thus immunohistochemistry for LC3 cannot be used on its own as evidence for alterations in autophagic flux without corroborative evidence from another technique[102].

1.8 Creating models of uraemia

The term 'uraemia' is used to describe the constellation of pathophysiological changes accompanying loss of kidney function, rather than just the accumulation of nitrogenous waste products in the blood. It is a heterogenous syndrome that includes hypertension, left ventricular hypertrophy (LVH), disturbances in bone biochemistry, vascular calcification, dyslipidaemia and anaemia. In addition, no single 'uraemic toxin' has been identified, therefore creating realistic *in vivo* and *in vitro* models of renal disease is challenging.

1.8.1 Cell culture models of uraemia

Several experimenters have attempted to create a 'uraemic milieu' by incubating cells in culture medium supplemented with serum from uraemic animals, with serum from non-uraemic animals used as a control[113]. Alternatively selected 'uraemic toxins', such as indoxyl sulphate (IS) can be used singularly or in combination to simulate the uraemic environment[114]. Whilst possibly less realistic than using serum (which may be more representative of the abnormal biochemistry to which cells are exposed in animals with CKD), the latter approach has the advantage of introducing fewer variables into the experimental system: this is especially important when studying autophagy, as any variation in glucose and amino acids, for example, will dramatically effect autophagy induction. Additionally, it has the advantage that any differences from the control are quantifiable.

1.8.2 Rodent models of uraemia

Our group uses two animal models that have been developed to reflect this phenotype. When assessing autophagy *in vivo* any model of disease potential confounders must be taken into account. For example, it is generally held that animals do not particularly enjoy certain experimental diets, and are thus relatively calorie-deprived compared to animals fed a control diet. As CR is a known autophagy-inducer adenine-fed animals may demonstrate more autophagy activity as a result of this, rather than of the disease process being studied itself.

Careful experimental design is thus required in order to isolate a particular variable's effect on autophagy.

1.8.2.1 Adenine diet model

Yokazawa *et al.* first described the use of supplemental adenine to generate a model of uraemia in 1986[115]. Following a diet supplemented with 0.75% adenine for 30 days rats developed a uraemic phenotype. Histological examination of the kidneys revealed granuloma around crystalline deposits in the tubules and interstitium, along with evidence of marked fibrosis. There was also evidence of microtubular obstruction and dilatation and, not uncommonly, hydronephrosis. Serum creatinine concentrations were over three times higher than that of controls at day 30, rising to almost five times higher on day 50. The animals died between day 40 and 65[115].

Adenine is metabolised to adenosine monophosphate (AMP) via the enzyme adenine phosphoribosyltransferase (APRT). AMP may be metabolised via adenosine, inosine, hypoxanthine, xanthine, urate, and finally excreted as alantoin[116]. APRT becomes saturated by excess adenine, which is then oxidised to 2,8-dihydroxyadenine via xanthine oxidase. The 2,8- dihydroxy-adenine is poorly soluble in the urine at a physiological pH, and precipitates out in the urine causing a crystal tubulopathy with microtubular obstruction and granulomatous interstitial nephritis, leading to renal failure[116].

1.8.2.2 5/6 nephrectomy model

This is created by a two-stage surgical procedure, whereby 2/3rd of one kidney is initially removed followed, two weeks later, by a contralateral nephrectomy (leaving 1/6th of the original nephron mass remaining). Histological examination of the remnant kidney shows hypercellular glomerular tufts, with expansion of the glomerular volume and tubular atrophy. The serum creatinine rise is less than that in the adenine diet model, but subtotal nephrectomy animals are significantly hypertensive, with left ventricular hypertrophy and myocardial fibrosis[117], arguably making the 5/6 nephrectomy model a better mimic of CKD in humans.

1.9 Summary

The molecular biology of ageing is extraordinarily complex, and remains incompletely understood. It is likely that, rather than operating in isolation, the 'hallmarks of ageing' are interlinked and interdependent, and the cellular, tissue and organismal changes that comprise the ageing phenotype are a synthesis of their effects. Of note, it is still largely unproven that any of these changes 'cause' ageing, or whether they are merely signs of the ageing process itself[2].

The striking similarities between the physiologically aged and uraemic phenotypes, whilst much commented upon, has been little investigated at a cellular nor molecular level. One of the cellular processes thought to be impaired in ageing, autophagy, also plays a role in

maintaining cellular bioefficiency and homeostasis, in optimisation of the immune response and in inflammation limitation. These functions are also seen to be depressed in patients with CKD. Cellular senescence, consequent to telomere attrition and non-telomeric stimuli, results in tissue dysfunction and loss of regenerative potential and a pro-inflammatory phenotype, all of which is also seen in uraemic patients. There is some, limited, evidence that autophagy and senescence may be altered in uraemic humans and animals, though this has not been derived from well controlled experimental models. Moreover, no causal relationship between altered autophagy and senescence and the uraemic phenotype has been defined.

Cardiac changes are amongst the most striking seen in both physiological ageing and end stage renal failure. These include loss of functioning cardiac myocytes and compensatory hypertrophy of remaining cells, myocardial fibrosis, and, as a result, thickening and stiffening of the myocardium[118,119]. Interestingly, the suggested driving forces for these changes are similar for both ageing and uraemia, with enhanced inflammatory activity and oxidative stress seen in both 'conditions'[119,120]. Moreover, cardiac death remains the single greatest cause of mortality in patients (adult and paediatric) with advanced kidney disease[121,122]. Whilst atherosclerotic coronary artery disease is more common in patients with CKD than in the unaffected population, cardiac death is more often arrhythmic or unexplained[121], likely due to stiffening of the heart and major vessels. Autophagy plays an important role in maintaining cardiac health in both physiological and pathological states, and declining autophagy[123] and increased senescence[18] are seen in the aged heart. Indeed, a causative role for both processes in cardiac failure in the elderly has been proposed[124,125]. Our group has an interest and experience in cardiac disease in uraemia, and has established an *in vivo* rat model of uraemic

cardiomyopathy[86]. Thus it seemed both useful and practicable to investigate the effect of uraemia on autophagy, senescence and ageing in the heart.

Assessing autophagy and senescence in uraemia is a challenging proposition. Uraemia itself is a constellation of widespread pathophysiological changes which are very hard to define and untangle, and even more so to recreate in a controlled experiment. Furthermore, both autophagy and senescence are difficult to detect, monitor and manipulate, and are affected by a multitude of different signalling pathways, thus defining the relationship between uraemia in isolation and autophagy and senescence requires careful experimental design and utilisation of several techniques to gain an accurate picture.

However, this is an important, fascinating and little explored area of medical science, and one worth persevering with: understanding the impact of chronic disease on ageing (and vice versa) is possibly the single biggest challenge faced in western healthcare systems because of our rapidly growing elderly populations. Discoveries in this field have the potential not only to determine changes in the way we treat sick and elderly people, but may lead to a paradigm shift in the way we view sickness and ageing, with profound socioeconomic implications.

1.10 Aim of this thesis

The aim of this thesis is to assess the effect of uraemia on autophagy and senescence in the heart, the nature of their relationship, and how this contributes to the pathologically aged cardiac uraemic phenotype, using *in vitro* and *in vivo* models of uraemia.

Chapter 2: Methods

All materials and reagents were obtained from Sigma-Aldrich Company, Poole, Dorset, UK unless stated otherwise.

2.1 Cell culture techniques

Rat BDIX heart myoblast cells (H9c2, Public Health England, Porton Down, Wiltshire, UK) were cultured and passaged on 75 cm^2 cell culture flasks using Dulbecco's Modified Eagle's Medium (DMEM) containing 1g/L (5.5 mM) glucose, L-glutamine, sodium bicarbonate and pyridoxine. This was supplemented with 10% by volume Foetal Calf Serum (FCS), and 100 U/mL penicillin, 100 μg/mL streptomycin and 0.25 μg/mL amphotericin B. Cells were cultured in a humidified incubator (95% air and 5% CO_2). When cells had reached 70-80% confluence they were suspended using 10 mL Trypsin-EDTA solution and centrifuged at 1000 *g* for 5 min. The cell pellet was resuspended in 1 mL of culture media and then added to 50 mL of culture medium. 2 mL of this suspension was added to each of 24 wells on 4 x 6 well culture plates. Cells were cultured in these wells until 70-80% confluent. Culture media was replaced every 24 h.

2.1.2 Chloroquine dosing

Chloroquine phosphate (Santa Cruz Biotechnology Inc., Santa Cruz, CA, USA) was dissolved in water to produce a 10 mM solution. Volumes of this solution were added to cell culture wells to achieve 10, 25, 50 and 100 μM concentrations. Reverse osmosis water was used to equalise the volume added between the experimental and control wells. Cells were cultured for a further 6 h prior to being lysed.

In all cell culture work described hereon in, experiments were performed in duplicate and chloroquine solution was added to one of each pair for a set time prior to lysis.

2.1.3 Rapamycin dosing

Rapamycin (Enzo Life Sciences, Exeter, Devon, UK) was dissolved in dimethyl sulfoxide (DMSO) (Fisher Scientific, Loughborough, Leicestershire, UK) to produce a 200 μM solution. Volumes of this solution were added to cell culture wells to achieve 100, 250, 500 nM and 1 μM concentrations. DMSO was used to equalise the volume added between wells and in control wells. Cells were cultured for a further 24 h prior to being lysed.

2.1.4 Glucose deprivation/supplementation

Glucose-free DMEM (Gibco, Life Technologies Ltd, Paisley, Scotland, UK) was supplemented with D-glucose to achieve concentrations of 5.5 and 25 mM. L-glucose was added to equalise overall concentrations of glucose between wells and in control wells, thereby acting as an osmotic control. Wells were washed three times with phosphate buffered saline (PBS) prior to experimental media being added, then cultured for a further 24 h prior to lysis.

2.1.5 Simulated uraemia

IS was dissolved in reverse osmosis water to make a 10 mg/mL stock solution. Volumes of this solution were added to cell culture wells to achieve 10, 25, 50, 100 and 200 μg/mL concentrations. Genetic grade water was used to equalise the volume added between wells and in control wells. Cells were cultured for a further 24 or 48 h prior to lysis.

2.2 Western blotting for markers of autophagic flux in rat BDIX heart myoblast cell cultures

2.2.1 Protein extraction

Media was removed from cell culture wells, which were then washed with 1 mL cold PBS. This was subsequently removed and 150 μL of protease inhibitor cocktail and protein extraction buffer mixture (GE Healthcare Life Sciences, Chalfont St Giles, Buckinghamshire, UK) in a 1:100 ratio added to each well. Adherent cells were systematically scraped from each well. Well contents were transferred to Eppendorf tubes (Eppendorf™, Hamburg, Germany) and centrifuged at 16,000 *g* for 10 min at 4°C. The supernatant from each Eppendorf tube was transferred to a fresh tube and placed on ice. From each sample 30 μL was removed and diluted in 30 μL reverse osmosis water and stored at –20 °C for protein quantification. The remaining sample was stored at -80°C.

2.2.2 Protein quantification

The protein content of cell lysates was calculated using a bicinchoninic acid (BCA) Protein Assay Kit (Pierce, Life Technologies Ltd) as per manufacturer's instructions.

2.2.3 Gel electrophoresis

26 μL of the sample with the lowest protein content was pipetted into an Eppendorf tube, along with 14 μL of a reducing agent (Invitrogen, Life Technologies) and NuPAGE LDS sample buffer (Novex™, Life Technologies) mixture (1:2.5 ratio). For other samples, the volume containing the same amount of protein as in 26 μL of the sample with the lowest protein content was calculated, and this was made up to 26 μL with genetic grade water. 14 μL of the reducing agent and sample buffer mixture was added as previously. Samples were denatured by heating at 99°C for 5 min, before being briefly centrifuged.

40 mL (20 x) of MOPS solution (Invitrogen, Life Technologies) was diluted in 760 mL genetic grade water to prepare a running buffer. To this was added 800 μL of antioxidant (Invitrogen, Life Technologies). A 12% NuPAGE Bis-Tris gel (Novex™, Life Technologies) was opened, the combs removed and the wells washed three times and then filled with MOPS running buffer. Gels were then placed into an X Cell II Blot Module (Invitrogen), which was then filled with MOPS so that the wells were covered and the exterior filled to 2/3 full. 20 μL of each sample was pipetted into individual wells alongside 5 μL of a rainbow marker (Amersham, GE Healthcare Life Sciences), then run at 200 V for 1 h.

2.2.4 Transferring

1 litre of transfer buffer was prepared using (for one membrane) 850 mL reverse osmosis water, 50 mL (20 x) NuPAGE transfer buffer (Novex™, Life Technologies), 100 mL methanol and 1 mL antioxidant. This was used to soak filter papers and blotting pads. A 0.45 μM pore size polyvinylidene fluoride (PVDF) membrane (Fisher Scientific) was pre-soaked in 100% methanol. The gel was carefully removed and placed on a filter paper, then placed in the blotting module according to the manufacturer's instructions. The gel/membrane/filter paper/blotting pad sandwich and outer module was filled with transfer buffer. This was then run at 30 V for 2 h.

2.2.5 Blocking and detection

The membrane was agitated for 30 min in 20 mL StartingBlock TBS Blocking Buffer (Thermofisher Scientific). This was then drained, and the membrane cut in half between 20 and 30 kDa, as determined from the rainbow markers. The lower portion was then agitated overnight at 4°C in 10 mL of anti-LC3B antibody (Cell Signaling, New England Biolabs (UK) Ltd, Hitchin, Herts, UK), and the upper in 10 mL of anti-SQSTM1/P62 antibody (Abcam, Cambridge, Cambridgeshire, UK), both diluted to a concentration of 1:1000 in blocking buffer. This was then drained and the membrane portions washed three times for 5 min in Tris-Buffered Saline and Tween (TBS-T). 1 L of TBS-T was made up as follows:

50mM Tris-HCl, pH8

150 mM NaCl

0.1% v/v Tween 20

The membrane was then agitated for 1 h in goat anti-rabbit antibody bound to horseradish peroxidase (Cell Signaling) at a dilution of 1:2000. A further three washes of TBS-T were performed, then protein bands visualised using ECL Prime Western Blotting Detection Reagent (GE Healthcare) on ECL X-ray film (GE Healthcare). Protein loading was checked using reprobed membranes blotting for GAPDH using 1:10,000 dilutions of both primary and secondary antibodies, and incubating the membrane for 10 min in each with washing steps as before.

2.2.6 Densitometry of western blots

Densitometry of western blots was performed using Image J (http://imagej.nih.gov/ij/). Protein expression was represented by dividing the density of the test protein band by that of its respective control band and plotting the result.

2.3 Rodent models of uraemia

All *in vivo* experiments were approved by the institutional ethics committee and performed under licence granted by the Home Office (UK) in accordance with the Animals (Scientific Procedures) Act 1986.

2.3.1 Adenine diet model

6-week-old Wistar rats (Charles River, Margate, Kent, UK) were housed in an animal house with a 12 h day-night cycle and had free access to water. After 1 week acclimatisation, during which time all animals were fed standard chow, animals were then either fed a standard pellet diet (Rat and Mouse No.1 Maintenance, Special Diet Services, Witham, Essex, UK) or standard pellet diet with the addition of adenine 0.75% (Rat and Mouse No.1 Maintenance + 0.75%, Special Diet Services). Animals were fed the adenine diet for 4 weeks to generate an uraemic phenotype. Animals were fed standard chow to generate a (non-uraemic) control group.

2.3.2 Sub-total (5/6) nephrectomy model

6-week-old Wistar rats (Charles River) were housed in an animal house with a 12 h day-night cycle and had free access to standard chow and water. All procedures were conducted using aseptic technique and all instruments were sterilized in an autoclave before use.

After 1 week acclimatisation rats were anaesthetised with inhaled 1.5% isofluran (Baxter, Newbury, Berkshire, UK). The fur on the left flank was shaved and a 1 cm incision was made just inferior to the lower margin of the rib cage. The flank musculature was blunt dissected and the parietal peritoneum was cut. The left kidney was then externalised through the incision. The perinephric fat and renal capsule were removed and an arterial clamp placed around the renal artery and vein. 3 sections of renal parenchyma were removed: the upper and lower poles and the lateral surface of the kidney. The arterial clip was removed and

pressure applied to cut surfaces to promote homeostasis. Once this was achieved the kidney was replaced in the abdominal cavity. 1 ml of sterile saline was instilled into the abdominal cavity to replace fluid losses. The muscular layers were stitched together with 4-0 polysorb braded suture (Covidien UK Commercial Ltd, Farnham, Surrey, UK), and the skin was closed using a Precise disposable skin stapler (Bunzl Healthcare, Enfield, UK). 0.03 mL of Vetegesic (Buprenorphine, Alstoe Animal Health, Sheriff Hutton, York, UK) was injected to provide post-operative pain relief. The rats were left to recover under a warming lamp and returned to their cages when fully awake.

2 weeks after the left subtotal nephrectomy, rats were anaesthetised as before, a right flank incision was made and the right kidney was externalised as was the left. The right renal artery and vein were tied off and the entire kidney was removed distal to the ties. The abdomen was sutured up, opiates were given and the animal was left to recover as before. The animals were then left for 4 weeks to develop a uraemic phenotype.

Control animals were created in a 2 stage, sham procedure, in which no renal tissue was removed from the left kidney and the right kidney was replaced in the abdominal cavity after it was decapsulated.

Achievement of uraemia was confirmed by serological testing of creatinine and urea concentrations at the time of sacrifice.

2.4 Rodent models of ageing

2 month and 24 month old C57BL/6 mice (Charles River) were housed in an animal house with a 12-hour day-night cycle and had free access to water.

2.5 GFP-LC3 transgenic mouse work

Transgenic green fluorescent protein (GFP)-LC3 mice (in which GFP has been tagged to LC3, allowing punctae associated with autophagosomes to be visualised under fluorescent microscopy) were kindly provided by Dr Norburu Mizushima at Tokyo Medical & Dental University, Japan (genetic background C57BL/6J).

Homozygote x heterozygote and homozygote x wild type systems were used to generate heterozygotes for experiment. Heterozygote x wild type was used when littermate controls were required. The PCR protocol below is currently unable to identify between wild type and heterozygote, therefore the use of florescence to detect GFP on ear samples prior to genotyping was implemented.

2.5.1 PCR protocol for genotyping GFP-LC3 mice

Primers 5' to 3'

Primer 1: ATAACTTGCTGGCCTTTCCACT

Primer 2: CGGGCCATTTACCGTAAGTTAT

Primer 3: GCAGCTCATTGCTGTTCCTCAA

Primers 1 + 2 = GFP-LC3 amplification

Primers 1 + 3 = Wild type Amplification

Reagents	Mix for N = 1
dH2O	15.90
NH4 buffer (10x)	2.50
MgCl2 (50mM)	1.75
dNTPs (10mM)	2.00
Primer 1 (100pM /µl)	0.20
Primer 2 (100pM /µl)	0.20
Primer 3 (100pM /µl)	0.20
Taq (5U/ul)	0.025
Total Volume	23.00

Step 1	4 min 94°C	
Step 2	30 sec 94°C	30 cycles
Step 3	30 sec 60°C	
Step 4	60 sec 72°C	
Step 5	7 min 72°C	

(PCR protocol for genotyping GFP-LC3 mice provided by Dr Mizushima)[126]

2.5.2 PCR results

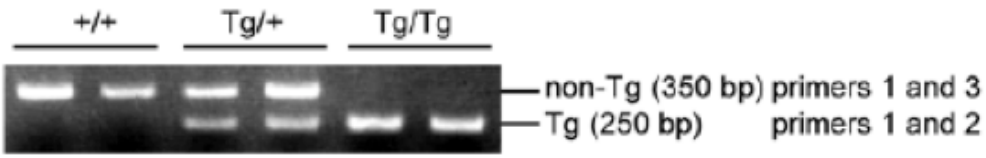

Kuma, A. and Mizushima, N., Autophagy 4:1, 61-62; 1 January 2008)

Figure 2: PCR result for genotyping GFP-LC3 mice (provided by Dr Mizushima)[126]

2.5.3 Adenine- versus control-diet mouse experiment

This was conducted in exactly the same way as the, previously described, rat adenine-/control-diet experiment, with both conditions performed in GFP-LC3 animals and wild types.

2.6 Tissue retrieval

If autophagic flux was to be assessed, all animals were fasted for 24 h prior to sacrifice, in an effort to control for the effects of nutrient intake on autophagy activation. 4 h prior to sacrifice half of the experimental and control groups received an intraperitoneal injection of 10 mg/kg chloroquine (Santa Cruz Biotechnology) in 0.9% saline for injection (Mölnlycke Health Care, Dunstable, Bedfordshire, UK).

All animals were killed by cardiac puncture under deep anaesthesia (ketamine/xylazine in a 2:1 ratio, 1.5 mL/kg, Link Pharmaceuticals, Horsham, West Sussex, UK). Tissues were retrieved and either snap frozen in liquid nitrogen (for western blotting, PCR or β-galactosidase staining) or immersed in 10% formalin for 24 h followed by 70% ethanol for immunohistochemistry.

2.7 Western blotting for markers of autophagic flux and senescence in rodent tissues

2.7.1 Homogenisation and protein extraction

Individual tissues were weighed and placed in an appropriately-sized vessel with 5 μL/mg radioimmunoprecipitation assay (RIPA) buffer and protease inhibitors:

Composition of RIPA buffer

50 mM Tris HCL (Fisher Scientific), pH 7.4

150 mM NaCl

1 mM ethylenediaminetetraacetic acid (EDTA)

1% v/v Triton X-100

0.5% v/v Na-deoxycholate

0.1% v/v sodium dodecyl sulphate (SDS)

Protease inhibitors (final concentrations)

1 μg/mL aprotinin

1 μg/mL leupeptin

1 mM phenylmethanesulfonylfluoride (PMSF)

1 mM NaF

1mM Na_3VO_4

This was placed in a beaker of ice water and the contents homogenized using an ultrasonic processor (Jencon's Scientific Limited, VWR, Lutterworth, Leicestershire, UK). Homogenate was allowed to stand on ice for 15 min and then centrifuged at 16,000 *g* for 10 min at 4°C. The supernatant was then removed and 150 μL aliquots frozen at -80 °C. Protein quantification and western blotting was carried out the same way as described previously. Primary antibodies for the autophagy markers LC3A/B and SQSTM1/P62, and the senescence markers p53, P21 and P15/16 were used.

2.8 Real-time PCR for expression of autophagy- and ageing-related genes in rat cardiac tissues

All reagents and materials for PCR were obtained from Qiagen, Manchester, Greater Manchester, UK unless stated otherwise.

Whole, snap-frozen cardiac tissue was transferred directly from liquid nitrogen into a liquid nitrogen-filled mortar, and ground to a fine powder using a liquid nitrogen-cooled pestle. 30 mg of powder was transferred into a liquid nitrogen-cooled cryovial, to which 300 μl Buffer RLT with 10 μL/mL β-mercaptoethanol (Sigma-Aldrich) was added. This suspension was homogenised by being passed 5 times back and forth through a 20 g needle (BD Medical, Fisher Scientific) using a 1 mL RNase-free syringe (BD Medical)

2.8.1 RNA extraction from rat cardiac tissue

RNA extraction was performed using Qiagen's RNeasy Fibrous Tissue Mini Kit as per the manufacturer's instructions.

2.8.2 Estimation of extracted RNA purity and quantity

RNA purity and quantity was initially estimated using a NanoDrop UV-Vis spectrophotometer (Thermo Scientific). A 260/280 nm ratio of ~ 2.0 was considered indicative of sufficient RNA purity to proceed.

2.8.3 Reverse transcription of extracted RNA

1 μg of extracted RNA was reverse transcribed to cDNA using Qiagen's RT2 First Strand Kit as per the manufacturer's instructions.

2.8.4 Real time PCR of cDNA for expression of autophagy- and ageing-related genes

Real time PCR of cDNA for 84 key autophagy- and ageing-related genes was performed using RT^2 SYBR Green ROX FAST Mastermix and species specific autophagy- and ageing-dedicated RT^2 Profiler PCR Arrays (Qiagen catalogue numbers PARN-084Z and PARN-178Z respectively, see Figure 6). Sample preparation was performed as per product literature. Arrays were run using a Corbett Rotor-Gene 6000 real-time PCR analyser using a profile specified by Qiagen's product literature.

2.8.5 Quality control and data analysis

PCR products were run on an agarose gel and the resultant bands checked with Qiagen (Figure 6, this was not recommended in Qiagen's product literature as the arrays already contain inbuilt checks for RNA quality, reverse transcription and PCR efficiency and genomic DNA contamination, but was undertaken as an additional quality control measure). A melt curve was also performed at the end of the run to exclude the presence of DNA contamination and primer-dimers (Figure 6).

Fold-change in gene expression between control and uraemic groups was calculated using the 2^(-ΔΔCt) method. This was done using Qiagen's online data analysis programme at http://pcrdataanalysis.sabiosciences.com/pcr/arrayanalysis.php

and subsequently checked manually. P values were calculated based on a Student's t-test of the replicate of 2^(-ΔCt) values for each gene in the adenine- and control-diet groups.

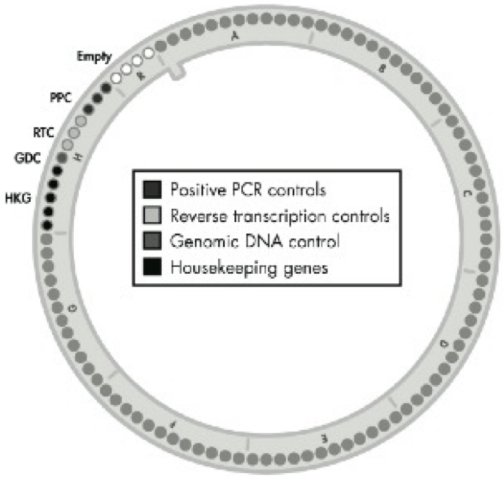

A

B

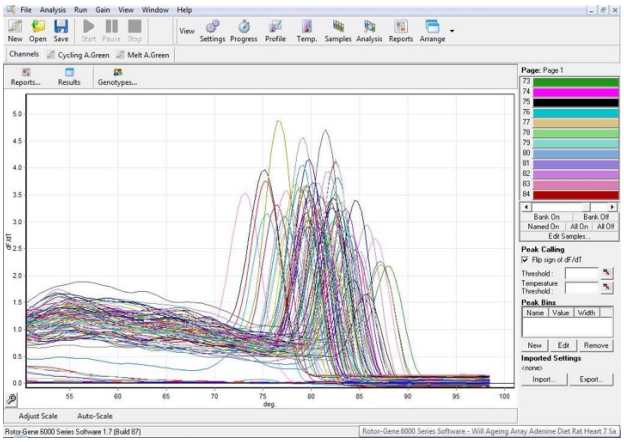

C

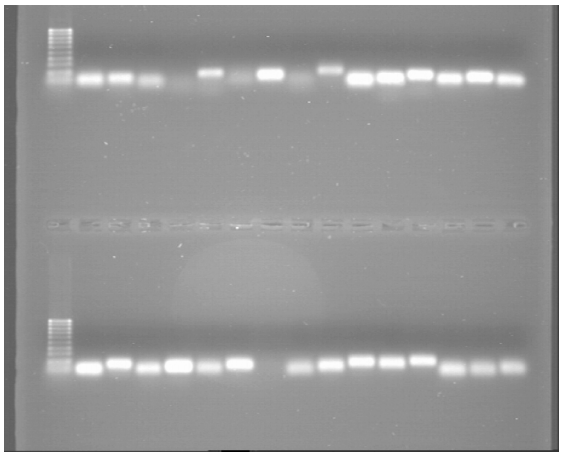

D

Figure 3: PCR array methodology and quality control. **A**: Diagram of generic 84 gene PCR array (Qiagen product literature). **B**: Photo of autophagy PCR array. **C**: Melt curve of PCR product in an ageing array **D**: Agarose gel electrophoresis of PCR product from an autophagy array from RNA extracted from cardiac tissue from an adenine-diet fed rat.

2.9 Histology

2.9.1 Immunohistochemistry

Tissues were harvested from animals and placed in 10% formalin for 24 h before being transferred into 70% ethanol in water. They were then processed by the Pathology Department of the Bart's Cancer Institute, Charterhouse Square. Samples were embedded in paraffin and sectioned using a microtome. Immunohistochemisty for LC3A, LC3B and p53 (all Cell Signaling, New England Biolabs (UK) Ltd) was performed using 1:100 antibody dilutions. Tissues were counterstained using haematoxylin and eosin.

2.9.2 Fixation and sectioning of GFP-LC3 murine tissue for fluorescent microscopy

Mice were anaesthetized as described previously. The heart was exposed by midline sternotomy, and 12 mL of chilled, 4% paraformaldehyde (PFA) in PBS infused into the left ventricle over 3 min via cardiac puncture. Tissues were subsequently excised and washed in 4% PFA, then immersed in 4% PFA overnight at 4˚C. Tissues were then immersed in 15% sucrose in PBS for 4 h, followed by 30% sucrose in PBS overnight. Tissues were embedded in optimal cutting temperature compound (O.C.T. compound – VWR International Ltd, Lutterworth, Leicestershire, UK), frozen on dry ice then kept at – 80 ˚C.

A Cryostat (Bright Instruments) was cooled to - 20 ˚C, and frozen, embedded tissues placed inside to reach this temperature. Tissues were mounted on the sectioning block using O.C.T., and sectioned at 5-7 μM. Sections were collected on glass slides and air dried at room

temperature for 30 min. They were then gently washed in PBS, excess PBS removed and DAPI Fluoromount-G® (SouthernBiotech, Cambridge Bioscience Ltd, Cambridgeshire, UK). Slides were mounted with cover slips and the edges sealed with nail varnish.

2.9.3 Fluorescence microscopy of GFP-LC3

Slides were viewed using a 60 x oil-immersion lens on a fluorescent microscope (Olympus), with GFP, RFP (red fluorescent protein) and DAPI (4', 6-diamidino-2-phenylindole) filter sets. Images were taken using the briefest possible fluorescent exposure to prevent photo breeching.

GFP-LC3 punctae were distinguished from autofluorescence signals by taking control images using a RFP filter set in addition to a GFP filter set. True GFP-LC3 signals were detected specifically by a GFP filter set.

2.9.4 Analysis of GFP-LC3 images

Images were analysed using a free, downloadable plugin for Image J (http://imagejdocu.tudor.lu/doku.php?id=macro:gfp-lc3_macro). Autophagy activity was assessed by the counting the average number of GFP-LC3 punctae per cell relative to controls.

2.9.5 Histochemical detection of SA-β-Gal

A Cryostat (Bright Instruments) was cooled to - 20 ˚C, and frozen, embedded tissues placed inside to reach this temperature. Tissues were mounted on the sectioning block using O.C.T, and sectioned at 4 µm. Sections were collected on glass slides and air dried at room temperature for 30 min, then fixed in 1% formalin in PBS at room temperature for 1 min. They were then gently washed in PBS and immersed overnight in β-Gal staining solution (supplied as part of Senescence Detection Kit, Abcam). Tissues were again washed with PBS, then counterstained with H&E and viewed under bright field at 100 – 200 x magnification.

2.10 Data analysis

Unless otherwise specified Mann-Whitney U test was used for all statistical analysis unless otherwise stated. $P < 0.05$ was considered significant.

Chapter 3: Results

3.1: Results of *in vitro* immunoblotting

3.1.1 The effect of chloroquine on autophagy in cultured H9c2 cells

It is necessary to determine a way of arresting autophagy at the autophagosomal stage, as this is required to gain an accurate impression of the extent of autophagy induction (without this it cannot be said that autophagy is being upregulated at the pre-autophagosmal stage, or being interrupted downstream from this, the latter, of course, representing overall inhibition of completed autophagy)[109].

Chloroquine accumulates in acidic lysosomes and increases the lysosomal pH. This inhibits lysosomal hydrolases and prevents autophagosomal fusion and degradation[127]. Chloroquine was added to H9c2 cell cultures in order to determine whether it could be used to arrest autophagic flux in H9c2 cells, and if so at what concentration range. Cells were grown to 70 % confluency in 6-well plates in full media, with chloroquine added to achieve concentrations of 10, 25, 50 and 100 μmol/L for the last 6 h of 24 h of incubation. LC3B and p62 were resolved by immunoblot (Figure 4).

Increasing the concentration of chloroquine in full media for the final 6 h of incubation resulted in an increase in the amount of LC3B-II and p62 detected in H9c2 cells. A concentration range of 10-25 μmol/L of was henceforth chosen for further work as the inhibitory effect of chloroquine on lysosomal degradation at this concentration has been

corroborated by other studies, as has its lack of toxicity over the given time period[128].

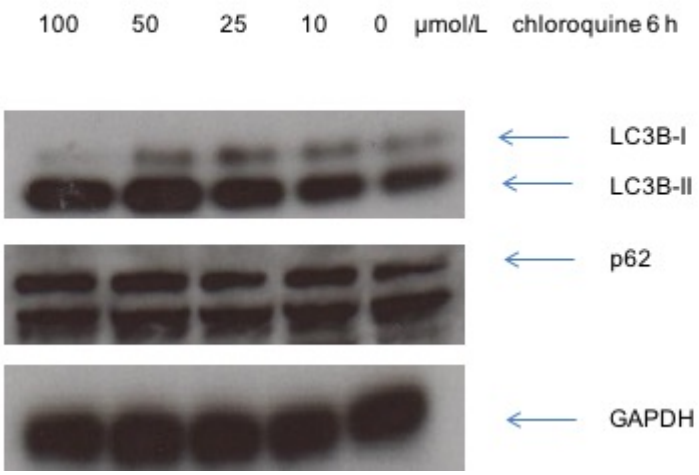

A

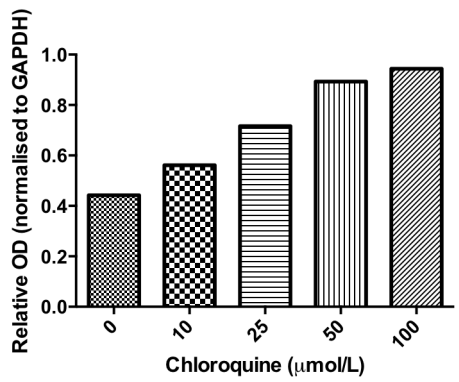

B

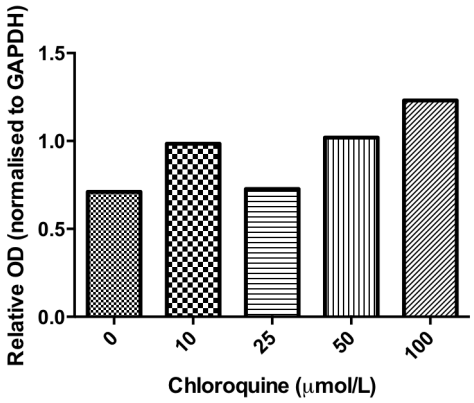

C

Figure 4: Effect of chloroquine on autophagy in H9c2 cells. **A**: Western blot showing bands reactive with LC3B, p62 and GAPDH at increasing doses of chloroquine (note: this p62 antibody additionally detects a lower, non-specific band). **B**: Graph showing densitometry of LC3BII band relative to that of GAPDH at increasing doses of chloroquine (n = 1). **C**: Graph showing densitometry of p62 relative to that of GAPDH at increasing doses of chloroquine (n = 1)

3.1.2 The effect of rapamycin on autophagy in cultured H9c2 cells

Rapamycin is known to upregulate autophagy via the mTOR pathway, has been demonstrated to prevent the development of uraemic cardiac hypertrophy[90], and is commonly used by clinicians as an immunosuppressant following organ transplantation[129]. It is thus useful as a 'positive control' for upregulated autophagy in cardiac myocytes.

H9c2 cells were grown to 70% confluency in 6-well plates in full media, whereupon rapamycin was added to achieve concentrations of 10, 25, 50 and 100 nmol/L for 24 h. Experiments were run in duplicate, and chloroquine added to one of each pair at a concentration of 25 μmol/L for the last 6 h of 24 h of incubation. LC3B and p62 were resolved by immunoblot (Figure 5).

Increasing the concentration of rapamycin increased the amount of LC3B-II detected in H9c2 cells up to a dose of 50 nmol/L. The amount of LC3B-II in H9c2 cells seemed to be greatest at the highest concentration of rapamycin tested (100 nmol/L, suggesting an indefinite dose-response effect), but in the presence of chloroquine this effect was reversed (there being less LC3B-II in cells exposed to rapamycin at this dose than in those exposed to none). It is thus possible to speculate that at very high concentrations rapamycin may actually inhibit autolysosomal degradation. Interestingly rapamycin seemed to have very little effect on the amount of p62 detected. One would expect the expression of p62 to reflect the upregulation of autophagy (and hence that of ubiquinated protein breakdown) by rapamycin (i.e. decreasing with increasing doses of rapamycin, an effect cancelled out or even reversed by the addition of chloroquine[113]).

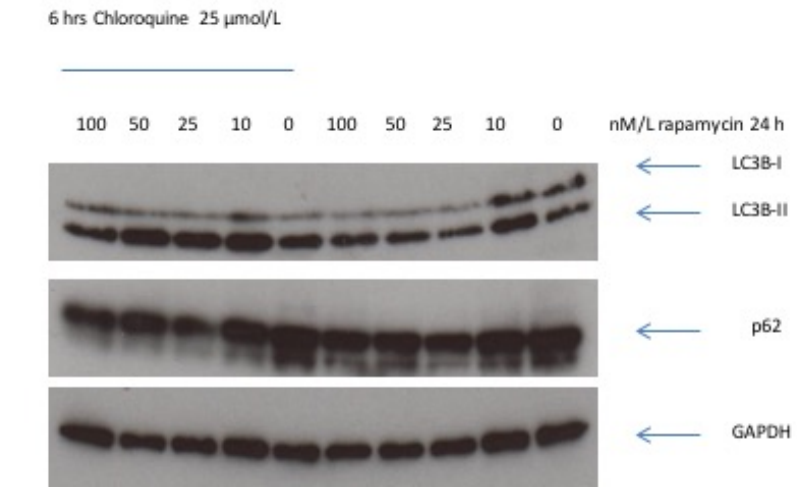

A

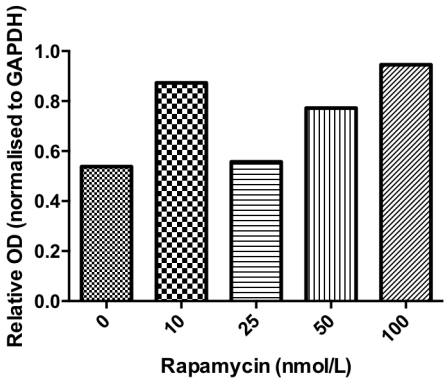

B

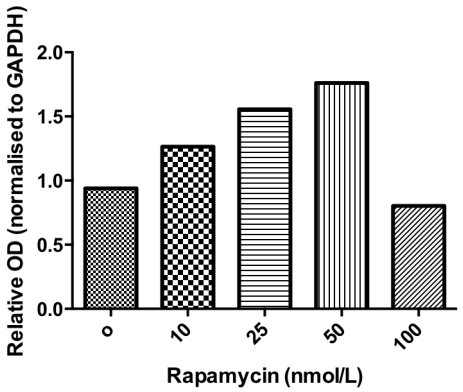

C

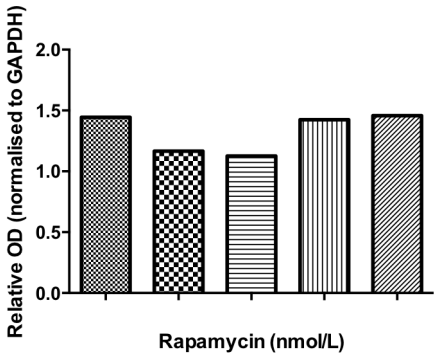

D

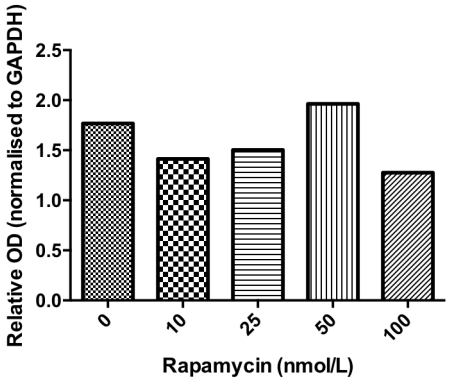

E

Figure 5: Effect of rapamycin on autophagy in H9c2 cells. **A**: Western blot showing bands reactive with LC3B, p62 and GAPDH at increasing concentrations of rapamycin after 24 h, with and without chloroquine. **B**: Graph showing densitometry of LC3BII band relative to that of GAPDH at increasing concentrations of rapamycin without chloroquine. **C**: Graph showing densitometry of LC3BII band relative to that of GAPDH at increasing concentrations of rapamycin with chloroquine. **D**: Graph showing densitometry of p62 band relative to that of GAPDH at increasing concentrations of rapamycin without chloroquine. **E**: Graph showing densitometry of p62 band relative to that of GAPDH at increasing concentrations of rapamycin with chloroquine. (n = 1 in all)

3.1.3 The effect of glucose on autophagy in cultured H9c2 cells

Nutritional status (and in particular levels of glucose and amino acids) is well established as one of the key determinants of autophagy activity, acting via the AMPK and mTOR pathways respectively[48]. Indeed, glucose-deprivation has been shown to induce autophagy in cultured cardiac myocytes, and has been used to mimic ischaemia in experimental models of cardiac insult[130]. Rodent models of uraemia are known to be anorexic and consequently nutritionally depleted, therefore it was important to assess the effect of this on autophagy in cardiac myocytes as a potential confounder which would need to be corrected for.

It was decided to investigate the effect of glucose on autophagy in cardiac myocytes in conditions of serum starvation: in addition to bovine serum albumin (BSA), FCS contains sugars which would confound attempts to assess the impact of total glucose deprivation. Moreover, FCS contains large quantities of diverse growth factors and cytokines, which may also affect autophagy.

H9c2 cells were grown to 70% confluency in 6-well plates in full media, whereupon media was replaced by glucose-free DMEM alone, with D-glucose added to achieve concentrations of 5 and 10 mM (L-glucose was used as an osmotic control) for 24 h. Experiments were conducted in fours, with chloroquine added to one of each four at a concentration of 25 µmol/L for the last 6 h of 24 h of incubation. LC3B and p62 were resolved by immunoblot (Figure 6).

In the absence of chloroquine, an increase in LC3BII in glucose-free cell culture suggested an upregulation of autophagy. However, it is important to note that p62 was also increased, suggesting that this increase may be due to an accumulation of autophagosomes that are not subsequently broken down, rather than an accelerated production. This seems to have been confirmed by running the same experiment with chloroquine, which produced a greater amount of LC3BII with than without glucose.

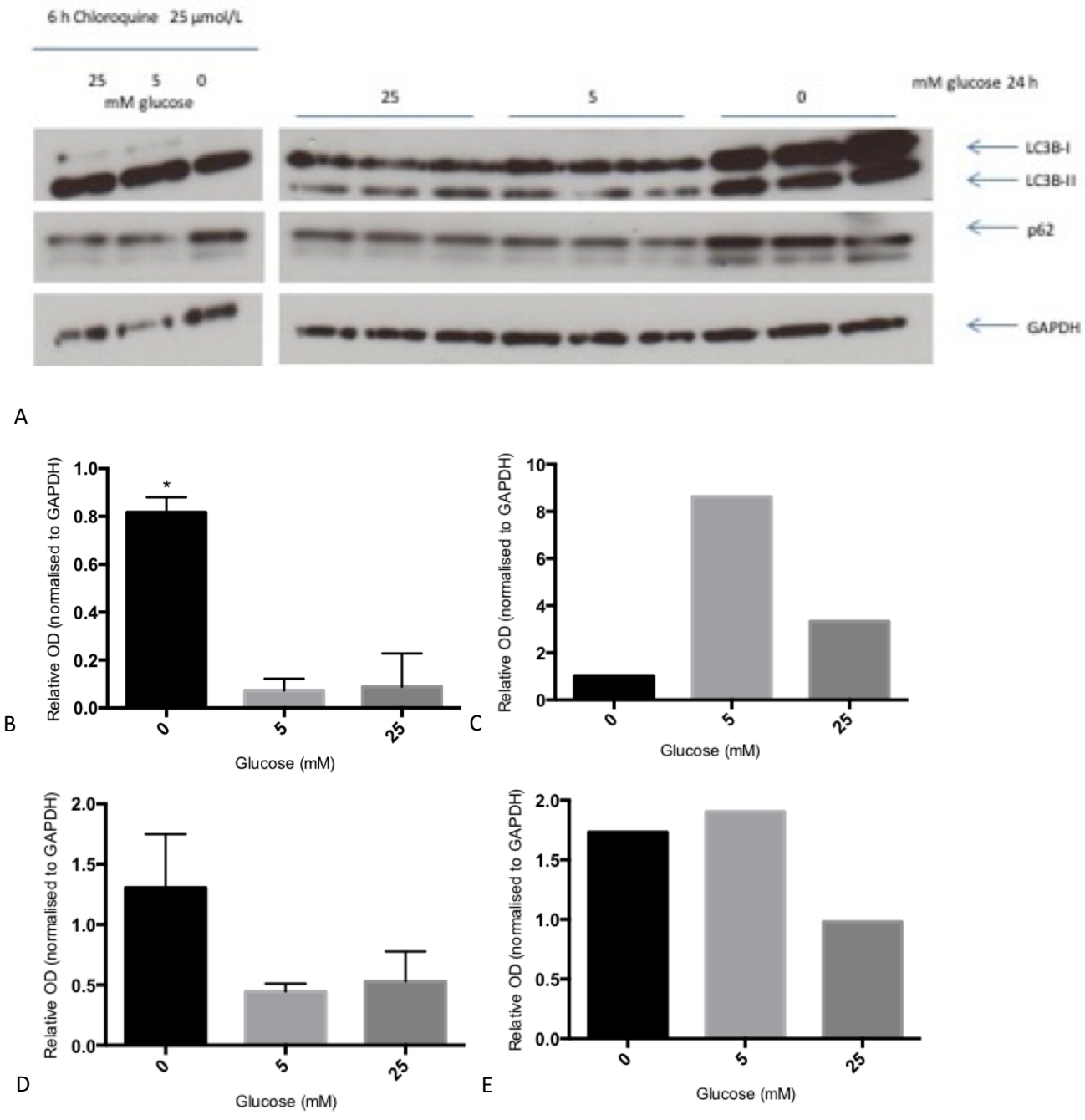

Figure 6. Effect of glucose on autophagy in H9c2 cells in the context of serum starvation. **A**: Western blot showing bands reactive with LC3B, p62 and GAPDH in amino acid and serum free media at increasing concentrations of glucose after 24 h, with and without chloroquine. **B**: Graph showing densitometry of LC3BII band relative to that of GAPDH at increasing concentrations of glucose without chloroquine (* denotes p value of 0.005 by Kruskal-Wallis, n=3). **C**: Graph showing densitometry of LC3BII band relative to that of GAPDH at increasing concentrations of glucose with chloroquine (n = 1). **D**: Graph showing densitometry of p62 band relative to that of GAPDH at increasing concentrations of glucose without chloroquine (n = 3). **E**: Graph showing densitometry of p62 band relative to that of GAPDH at increasing concentrations of glucose with chloroquine (n = 1).

3.1.4 The effect of indoxyl sulphate on autophagy in cultured H9c2 cells

A particularly well-validated uraemic toxin is indoxyl sulphate (IS), which results from protein fermentation in the large intestine. Colonic microbiota degrade tryptophan to indole, which is absorbed from the gut into the portal circulation. This is further metabolised to IS by the liver before being released into the systemic circulation. Free IS is excreted by the kidneys, and is thus retained in CKD, and is poorly removed by conventional haemodialysis due to its high binding affinity for albumin. Rising serum levels of IS are associated with vascular disease and mortality in CKD patients[131].

H9c2 cells were grown to 70% confluency in 6-well plates in full media, whereupon indoxyl sulphate was added to achieve concentrations of 10, 25, 50, 100 and 200 μg/mL for 24 h and 48 h. Experiments were run in duplicate, with chloroquine added to one of each pair at a concentration of 10 μmol/L for the last 4 h of incubation. LC3B and p62 were resolved by immunoblot (Figures 7 and 8).

Incubating cells in media containing increasing concentrations of indoxyl sulphate for 24 h produced a concentration-dependent increase in the amount of LC3B-II up to and including a dose of 50 μg/mL, suggesting an increase in autophagy initiation (Figure 7). This was corroborated by the addition of chloroquine, which did not reverse the pattern, thus confirming that the accumulation of LC3B-II was due to increased autophagy stimulation rather than the interruption of lysosomal breakdown of autophagic cargo. This effect was not

seen in p62 detection, thus it is tempting to speculate that over this time period IS stimulated an increase in autophagy, but not the successful breakdown of ubiquinated proteins.

Incubating cells in media containing the same concentrations of indoxyl sulphate for 48 h resulted in a similar pattern of LC3B-II detection, with the amount of LC3B-II particularly elevated in cells exposed to 25 μg/mL IS in the presence of chloroquine and decreasing somewhat above this (Figure 8). Interestingly, at 48 h clearance of p62 was increased with increasing concentrations of IS up to 50 μg/mL, with levels tending to be lower in cells not exposed to chloroquine (suggesting completed removal by autophagy), a pattern reversed by the addition of chloroquine (confirming that autophagy initiation had indeed been increased rather than lysosomal function inhibited.

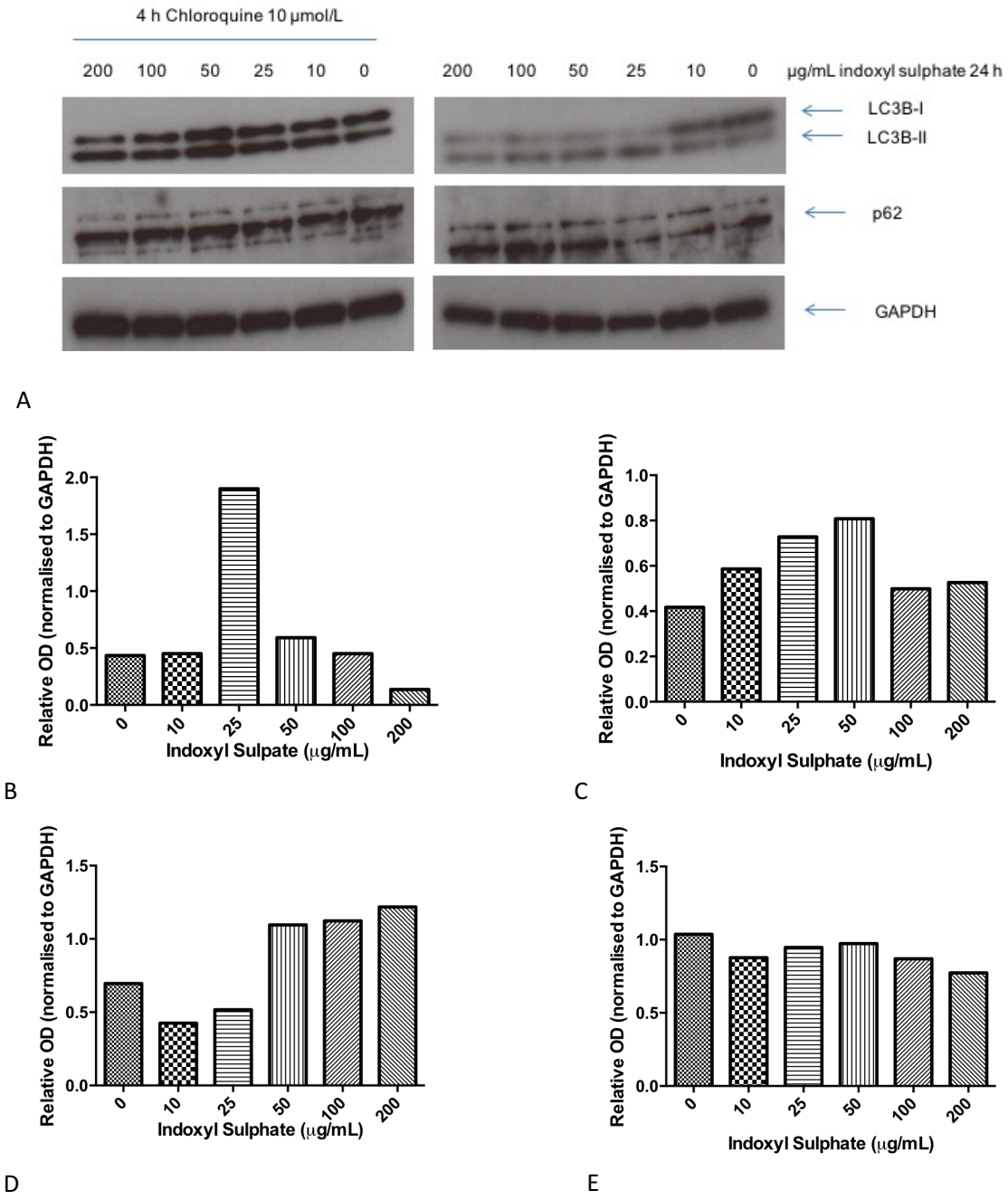

Figure 7. Effect of indoxyl sulphate on autophagy in H9c2 cells at 24 h. **A**: Western blot showing bands reactive with LC3B, p62 and GAPDH at increasing concentrations of indoxyl sulphate for 24 h, with and without chloroquine. **B**: Graph showing densitometry of LC3BII band relative to that of GAPDH at increasing concentrations of indoxyl sulphate at 24 h without chloroquine. **C**: Graph showing densitometry of LC3BII band relative to that of GAPDH at increasing concentrations of indoxyl sulphate at 24 h with chloroquine. **D**: Graph showing densitometry of p62 band relative to that of GAPDH at increasing concentrations of indoxyl sulphate at 24 h without chloroquine. **E**: Graph showing densitometry of p62 band relative to that of GAPDH at increasing concentrations of indoxyl sulphate at 24 h with chloroquine. (n = 1 in all)

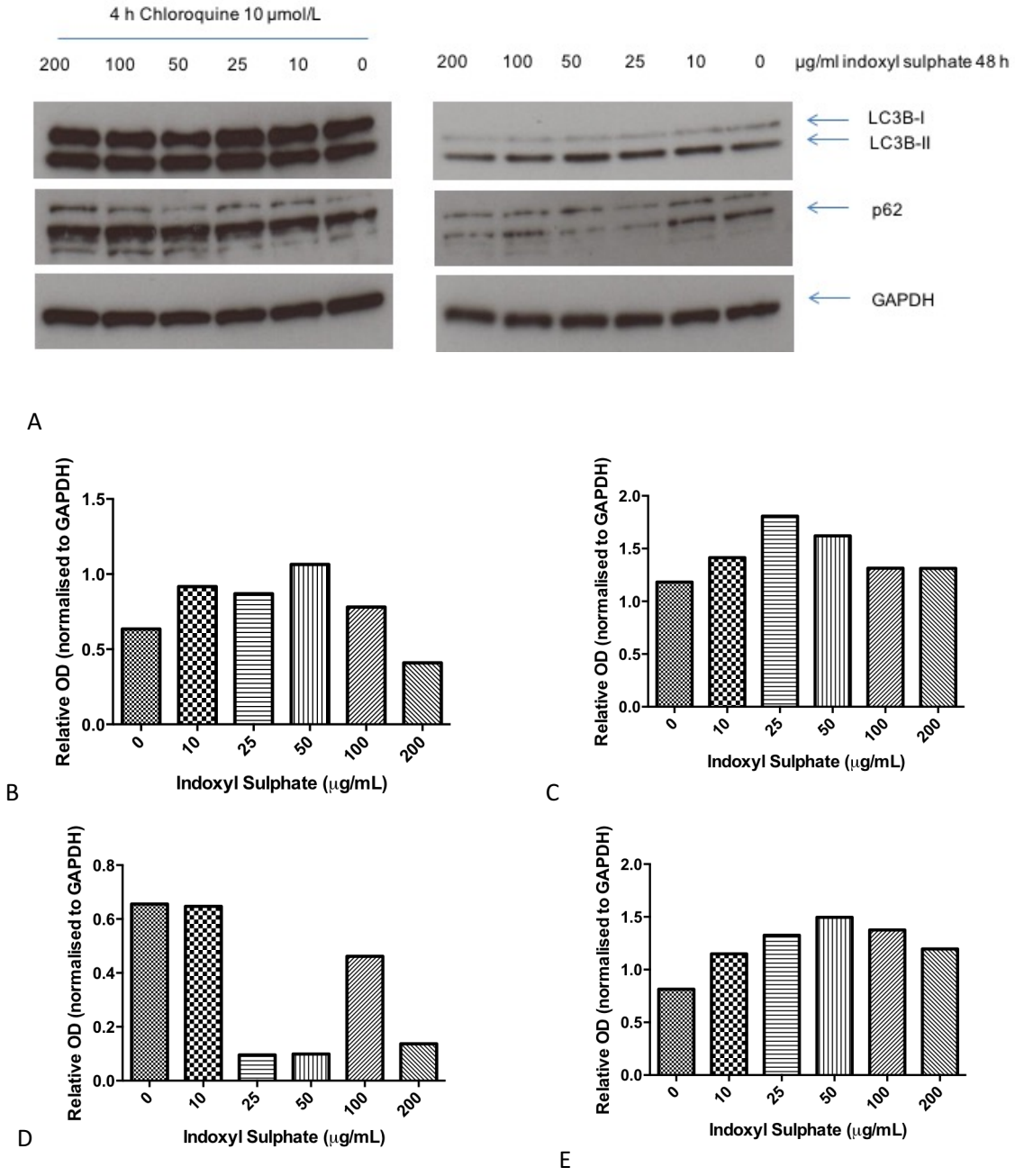

Figure 8: Effect of indoxyl sulphate on autophagy in H9c2 cells at 48 h. H9c2 cells were grown in full media, to which indoxyl sulphate was added to achieve the above concentrations for 48 h. Chloroquine was added to one of each group at a concentration of 10 µM/L for the last 4 h of incubation. Proteins were resolved by immunoblot. **A**: Western blot showing bands reactive with LC3B, p62 and GAPDH at increasing concentrations of indoxyl sulphate after 48 h, with and without chloroquine. **B**: Graph showing densitometry of LC3BII band relative to that of GAPDH at increasing concentrations of indoxyl sulphate at 48 h without chloroquine. **C**: Graph showing densitometry of LC3BII band relative to that of GAPDH at increasing concentrations of indoxyl sulphate at 48 h with chloroquine. **D**: Graph showing densitometry of p62 band relative to that of GAPDH at increasing concentrations of indoxyl sulphate at 48 h without chloroquine. **E**: Graph showing densitometry of p62 band relative to that of GAPDH at increasing concentrations of indoxyl sulphate at 48 h with chloroquine (n = 1 in all)

3.1.5 Discussion

These, *in vitro*, experiments confirmed that autophagy could be assayed and manipulated in a cardiac myoblast cell line, and that chloroquine was effective at arresting autophagic flux, thus providing a means of monitoring the degree of autophagy induction. It should be emphasised that these *in vitro* experiments involved limited numbers and thus statistical significance can largely not be attributed to their results.

Rapamycin treatment upregulated autophagy, confirming that autophagy can be stimulated in cardiac myocytes by mTOR inhibition: this was of great significance to further experiments, as it meant that anything influencing the mTOR pathway (e.g. nutritional intake) would have to be controlled for if possible, or at least taken into consideration in the analysis. Secondly it raises interesting questions with regards to the potential added beneficial effects of rapamycin (also known as sirolimus and marketed under the trade name Rapamune) after renal transplantation. Whilst animal experiments have suggested that the drug may prevent uraemic cardiac hypertrophy via inhibition of the mTOR pathway[90], no such studies have been done in humans.

Glucose deprivation in the context of serum starvation appeared to inhibit autophagy. This is an interesting finding (one might expect the reverse), and is corroborated by the work of Ramirez-Peinado *et al.*, who found that depriving cells of glucose did not cause them to engage in pro-survival autophagy[132]. The authors point out that previous groups claiming an autophagy-inducing role for glucose had deprived cells of other factors (such as serum)

simultaneously relative to the control environment, and it might be the absence of these other factors that had caused autophagy to be apparently upregulated rather than that of glucose. They also suggest that this is the case because completed autophagic degradation is an ATP-dependent process[132]. In the work presented here serum was removed, and hence growth factors, but this also happened to the control group, thus glucose concentration was the only variable. Other authors have suggested that in starvation conditions glucose actually induces autophagy via a p38 MAPK-dependent pathway[133].

Again, this was of great significance to further experiments, as it meant that anything influencing the AMPK pathway (e.g. nutritional intake) would have to be controlled for if possible, or at least taken into consideration in the analysis.

IS (an established uraemic toxin) appeared to stimulate autophagy, with the greatest difference versus control noticeable at 48 h with 25 μg/ml of IS. Interestingly, this is a level detectable in the plasma of dialysis patients[134]. Whilst not wholly representative of the 'uraemic milieu' cells are exposed to *in vivo*, this experiment provides a controlled demonstration of autophagy-upregulation by immortalized cardiac myoblasts when exposed to a substance known to accumulate in CKD.

3.2 Comparison of serum creatinine and urea in control, adenine-diet and 5/6 nephrectomy rats

Rodent models of uraemia were created using methodology described in Chapter 3, 3.3, page 58. All animals were fasted for 24 h (to correct for differences in caloric intake) and given chloroquine 10 mg/kg i.p. 4 h prior to sacrifice.

Both adenine-diet and 5/6 nephrectomy rats had significantly higher serum urea and creatinine levels than controls (Figure 9). As previously described, adenine-diet animals were significantly more biochemically 'uraemic' than those which had undergone 5/6 nephrectomy[86].

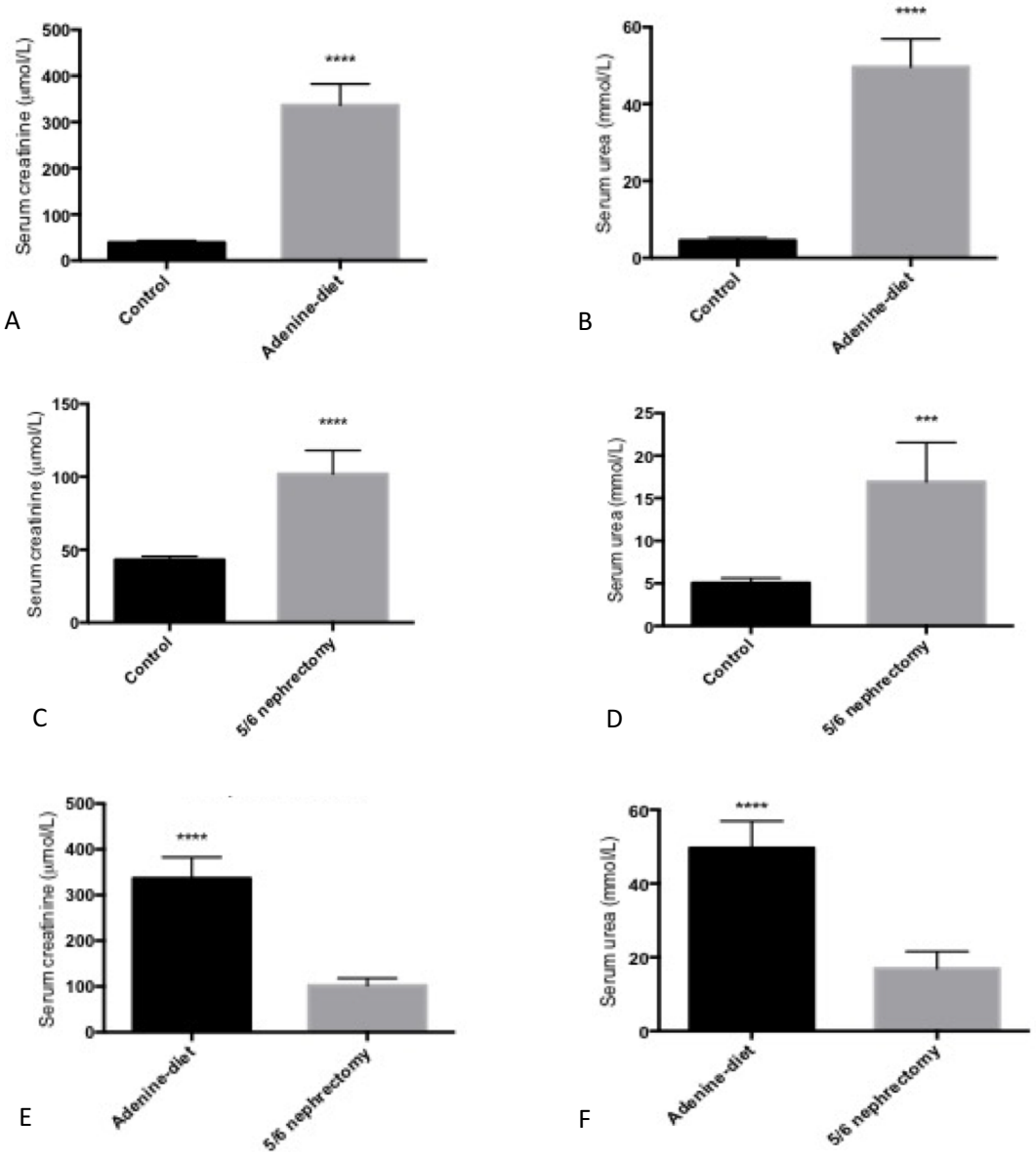

Figure 9: Serum urea and creatinine levels in control, adenine-diet and 5/6 nephrectomy rats. **A**: Serum creatinine in control and adenine-diet rats (**** denotes p value < 0.0001 by unpaired t test, n = 6). **B**: Serum urea in control and adenine-diet rats (**** denotes p value < 0.0001 by unpaired t test, n = 6). **C**: Serum creatinine in control and 5/6 nephrectomy rats (**** denotes p value < 0.0001 by unpaired t test, n = 5 and 8). **D**: Serum urea in control and 5/6 nephrectomy rats (*** denotes p value < 0.0002 by unpaired t test, n = 5 and 8). **E**: Serum creatinine in adenine-diet and 5/6 nephrectomy rats (**** denotes p value < 0.0001 by unpaired t test, n = 6 and 8). **F**: Serum urea in adenine-diet and 5/6 nephrectomy rats (**** denotes p value < 0.0001 by unpaired t test, n = 6 and 8).

3.3: Results of *in vivo* immunoblotting

3.3.1 The effect of uraemia on autophagy in adenine-diet rat hearts

Animals were fed either a control diet or adenine diet before being fasted for 24 h, with chloroquine 10 mg/kg i.p. given 4 h before being sacrificed. Cardiac tissue was harvested and snap frozen. Uraemia was confirmed by serological testing. LC3A and B, p62 and beclin 1 were resolved by immunoblot (Figure 10).

More LC3B-II was detected in the cardiac tissue of rats rendered uraemic using an adenine diet, fasted for 24 h and given chloroquine than in those with normal renal function previously fed a control diet. This did not reach statistical significance using densitometry. This was also visually true for LC3A-II (another isoform of LC3) and beclin-1 (a key protein involved in assembly of the autophagy machinery). Interestingly, less p62 was detected in the hearts from uraemic than that found in control rats (as measured by densitometry). This may not necessarily be a contradictory result (if accurate), as it may reflect incomplete blockade of autophagy by chloroquine (thus the greater levels of LC3A and B-II and beclin-1, and lower levels of p62, may actually represent increased autophagosome formation and increased breakdown of cargo proteins).

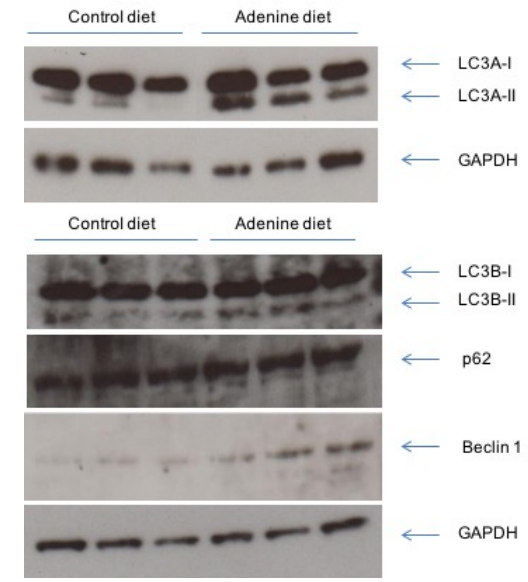

A

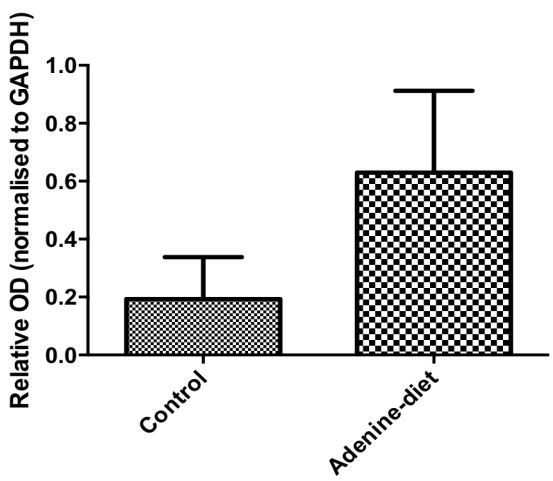

B

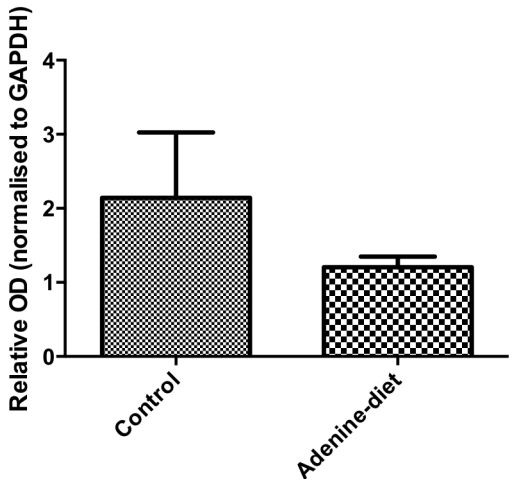

C

Figure 10: Autophagy activity in cardiac tissues of adenine-diet rats compared to controls. A: Western blots showing bands reactive with LC3A and B, p62, beclin 1 and GAPDH in protein isolates of cardiac tissues from control and adenine diet rats. **B**: Graph showing densitometry of LC3BII band relative to that of GAPDH in protein isolates of cardiac tissues from control and adenine diet rats (n = 3). **C**: Graph showing densitometry of p62 band relative to that of GAPDH in protein isolates of cardiac tissues from control and adenine diet rats (n = 3).

3.3.2 The effect of uraemia on autophagy in 5/6 nephrectomy rat livers

Cardiac tissues in the 5/6 nephrectomy rats were found to be very fibrous, and this presented difficulties in extracting and resolving small molecular weight proteins such as LC3B: I have thus included data from hepatic tissue here.

5/6 nephrectomy and sham procedure control rats were created using methodology described in Chapter 3, 3.3, page 58. Both groups were fasted for 24 h, with chloroquine 10 mg/kg i.p. given 4 h before sacrifice. Hepatic tissue was harvested and snap frozen. Uraemia was confirmed by serological testing. LC3A and B, p62 and beclin 1 were resolved by immunoblot (Figure 11).

More LC3B-II was detected in the hepatic tissue of rats rendered uraemic by 5/6 nephrectomy, fasted for 24 h and given chloroquine than in those with normal renal function who had undergone a sham procedure ($p = 0.029$ by Mann-Whitney U test, $n = 4$). This was also visually true for LC3A-II (another isoform of LC3). More p62 was also detected in 5/6 nephrectomy rat hepatic tissues, though this did not reach statistical significance. These findings suggest increased autophagy initiation in the hepatic tissues of 5/6 nephrectomy rats.

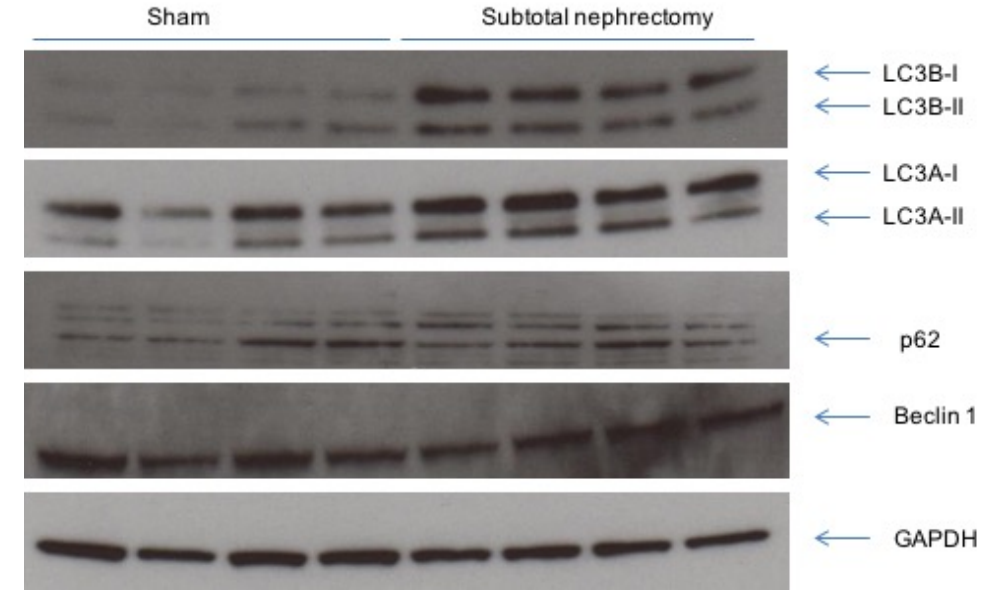

A

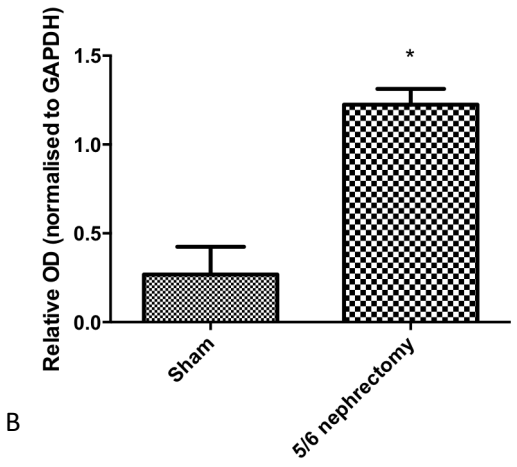

B

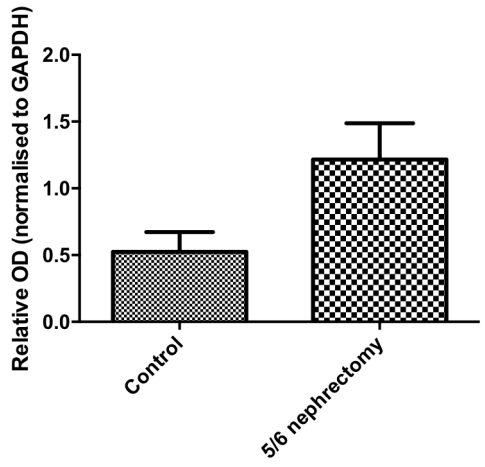

C

Figure 11: Autophagy activity in hepatic tissues of 5/6 nephrectomy rats compared to sham-operated controls. Animals underwent 5/6 nephrectomy or sham procedure before being fasted for 24 h, with chloroquine 10 mg/kg i.p. given 4 h before being sacrificed. Hepatic tissue was harvested and snap frozen. Uraemia was confirmed by serological testing. Proteins were resolved by immunoblot. **A**: Western blot showing bands reactive with LC3A and B, beclin 1, p62 and GAPDH in protein isolates of hepatic tissues from fasted 5/6 nephrectomy and sham-operated (control) rats. **B**: Graph showing densitometry of LC3BII band relative to that of GAPDH in protein isolates of hepatic tissue from fasted 5/6 nephrectomy and sham-operated (control) rats (∗ denotes p value of 0.029 by Mann-Whitney U test, n = 4). **C**: Graph showing densitometry of p62 band relative to that of GAPDH in protein isolates of hepatic tissue from fasted 5/6 nephrectomy and sham-operated (control) rats. (n = 4)

3.3.3 Markers of senescence in geriatric mice

It was necessary to establish the pattern of expression of established markers of senescence in chronologically elderly animals. These acted as a 'positive control' to which uraemic animals could be compared, as well as assessing the reliability of the antibodies. 24-month old mice were used, primarily due to availability and cost, though markers of senescence are conserved throughout rodent species.

24-month and 2-month old mice were fasted for 24 h, with chloroquine 10 mg/kg i.p. given 4 h before being sacrificed. Cardiac (and in this case hepatic) tissues were harvested and snap frozen. p53 and $p16^{Ink4a}$ were resolved by immunoblot (Figure 12).

The expression of p53 and $p16^{Ink4a}$ was significantly increased in the heart of 24-month compared to 2-month old mice (in fact these markers of senescence were barely detectable in the latter). The expression of p53 was significantly increased in the liver of 24-month compared to 2-month old mice; it is highly probable that $p16^{Ink4a}$ is also increased in elderly mouse hepatic tissues, but my attempts to demonstrate this were thwarted by difficulties with the antibody and the availability of tissues.

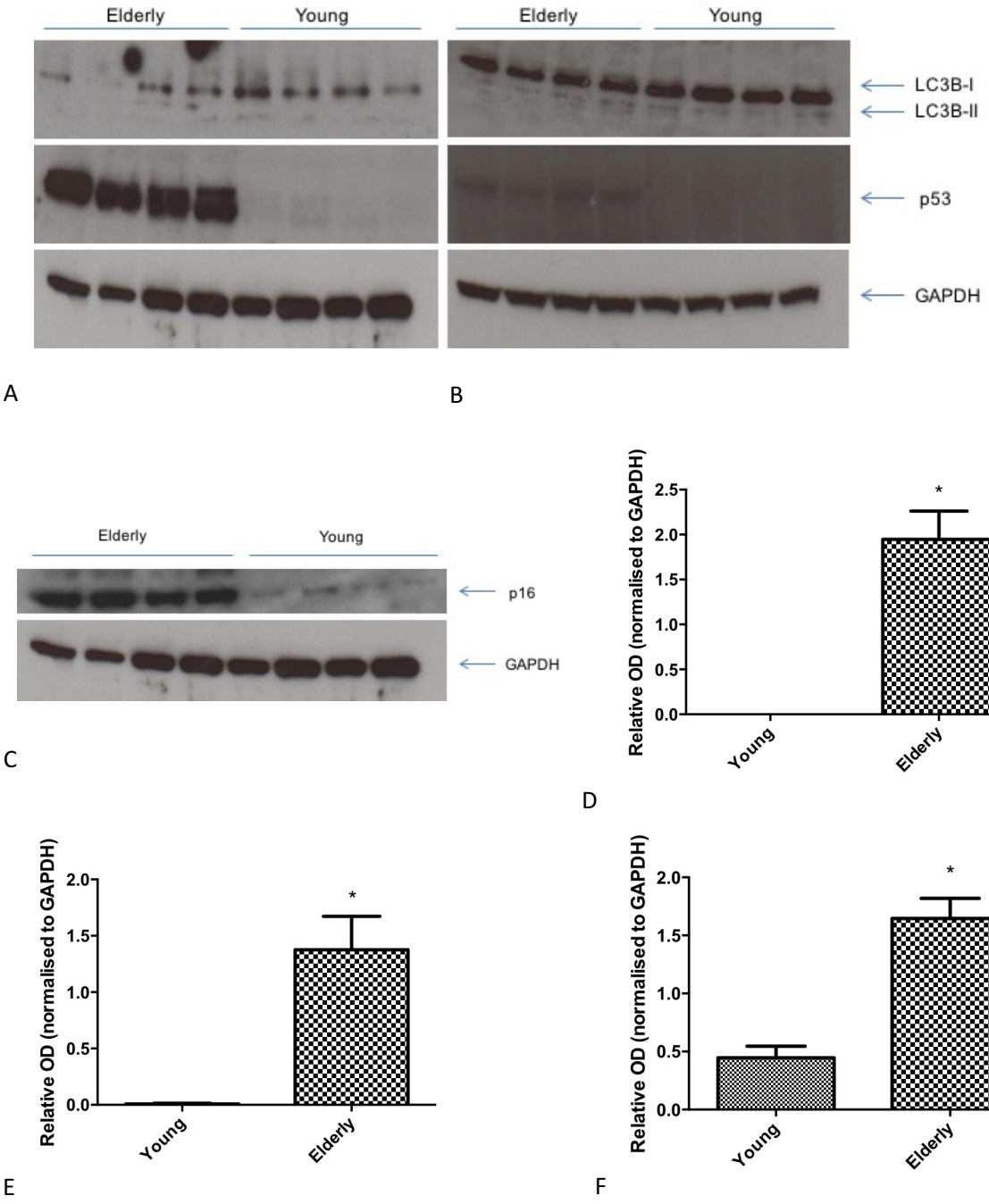

Figure 12: Markers of senescence in cardiac and hepatic tissues of elderly and young mice. **A**: Western blot showing bands reactive with p53 and GAPDH in protein isolates of cardiac tissues from fasted young and elderly mice. **B**: Western blot showing bands reactive with p53 and GAPDH in protein isolates of liver tissues from fasted young and elderly mice. **C**: Western blot showing bands reactive with $p16^{Ink4a}$ in protein isolates from cardiac tissues from fasted young and elderly mice. **D:** Graph showing densitometry of p53 band relative to that of GAPDH in protein isolates of cardiac tissue from fasted young and elderly mice (∗ denotes p value of 0.021 by Mann Whitney U test, n = 4). **E**: Graph showing densitometry of $p16^{Ink4a}$ band relative to that of GAPDH in protein isolates of cardiac tissue from fasted young and elderly mice (∗ denotes p value of 0.028 by Mann Whitney U test, n = 4). **F**: Graph showing densitometry of p53 band relative to that of GAPDH in protein isolates of hepatic tissue from fasted young and elderly mice (∗ denotes p value of 0.028 by Mann Whitney U test, n = 4).

3.3.4 The effect of uraemia on markers of senescence in adenine-diet rat hearts

Animals were fasted for 24 h, with chloroquine 10 mg/kg i.p. given 4 h before being sacrificed. Cardiac tissues were harvested and snap frozen. p53 and p15/p16 were resolved by immunoblot (Figure 13).

Whilst, visually, p53 expression seems to have been greater in cardiac tissue from adenine-diet rats (indicating greater senescence), this did not reach statistical significance using densitometry. There was no difference in p15/p16 expression, though this antibody did not seem as specific as the one used in the geriatric mouse experiment (which I was unfortunately unable to successfully employ here).

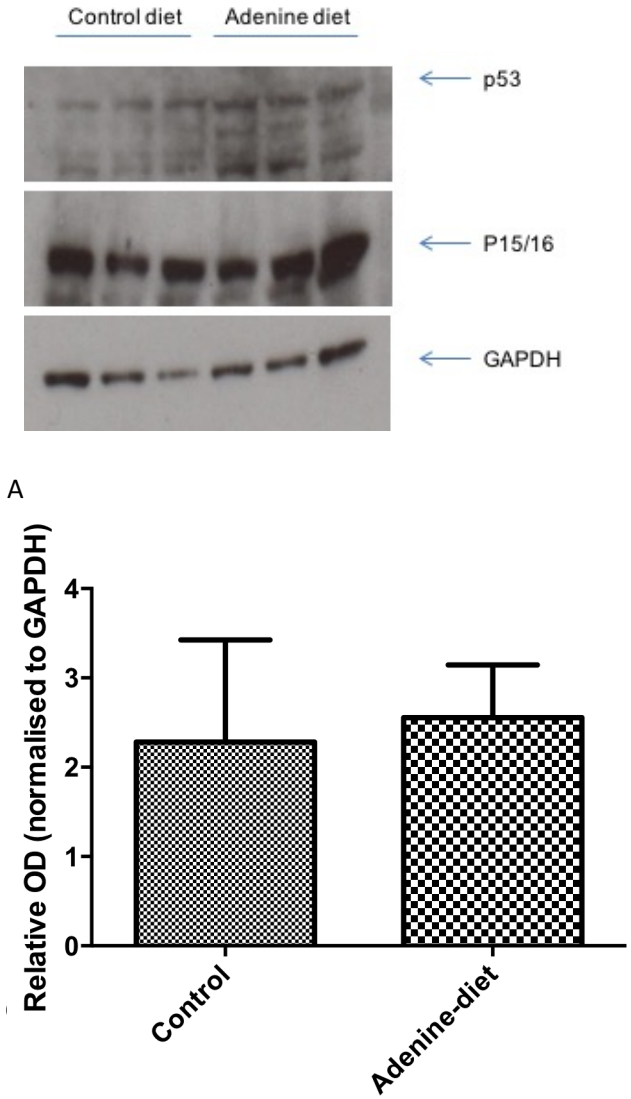

Figure 13: Markers of senescence in cardiac tissues in adenine diet and control rats. **A**: Western blot showing bands reactive with p53, p15/16 and GAPDH in protein isolates of cardiac tissues from fasted adenine diet and control diet mice. **B**: Graph showing densitometry of p53 band relative to that of GAPDH in protein isolates of cardiac tissue from fasted adenine diet and control rats (n = 3).

3.3.5 Discussion

Whilst not achieving statistical significance, LC3B-II (and LC3A-II and beclin-1) expression appeared greater in cardiac tissues from adenine-diet rats than controls. This suggests an increase in autophagic flux in the uraemic heart. Similarly, significantly more LC3A-II and LC3B-II was detected in the hepatic tissue of rats rendered uraemic by 5/6 nephrectomy (as seen in section 3.3.2), supporting the idea of an increase in autophagy in uraemia.

The expression of p53 and $p16^{Ink4a}$ was dramatically increased in the hearts of 24-month old mice compared to, confirming their usefulness as markers of senescence. The expression of p53 did not differ significantly in the hearts of adenine-diet and control rats. This could be taken to mean that there was no difference in senescence in the uraemic animals. However, p53 is not the only, nor the most specific, marker of senescence, therefore this result does not exclude an increase or decrease in senescence in the uraemic heart.

3.4: Autophagy- and Ageing-Related PCR arrays

3.4.1 The effect of uraemia on autophagy-related gene transcription

Autophagy is a complex process, which is affected by many signalling pathways, and involves numerous subcellular molecules and organelles that are temporally and spatially separated. There is thus little consensus or evidence for any one gene being more important than others, nor for reflecting a change in autophagy activity[108]. For these reasons autophagy transcription was assessed in adenine- and control-diet rat hearts using a previously validated[135], commercially available PCR array of 84 autophagy-related genes.

RNA was purified from snap-frozen cardiac tissues obtained from rats fed an adenine supplemented diet and a control diet and reverse transcribed, and real-time PCR performed using a commercially available array. Fold-change in gene expression between groups was calculated using the 2^(-ΔΔCt) method (Figure 14).

Autophagy-related gene expression did not differ greatly between adenine-diet and control rat hearts, only two genes showing a greater than twofold difference in expression. *Cxcr4* was expressed - 2.58 fold less in the adenine-diet hearts ($p = 0.019958$ by Student's t-test), and *Bcl2l1* + 2.67 fold more ($p = 0.0005$).

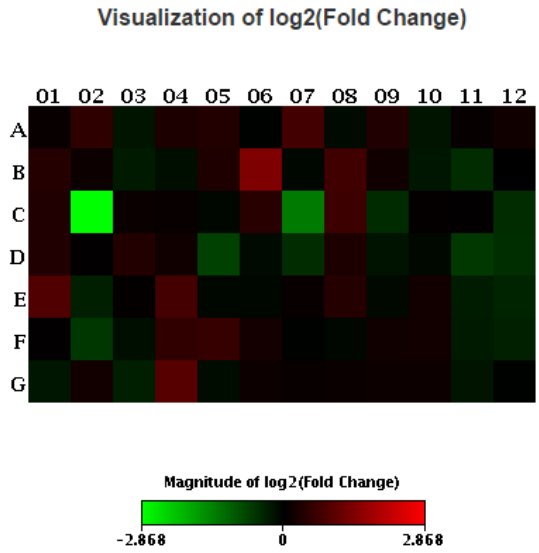

A

Layout	01	02	03	04	05	06	07	08	09	10	11	12
A	Akt1 1.06	Ambra1 1.44	App -1.17	Arsa 1.25	Atg12 1.30	Atg16l1 -1.01	Atg16l2 1.68	Atg3 -1.08	Atg4b 1.28	Atg4c -1.16	Atg5 1.04	Atg7 1.13
B	Atg9a 1.32	Bad 1.09	Bak1 -1.22	Bax -1.11	Bcl2 1.27	Bcl2l1 2.67	Becn1 -1.05	Bid 1.66	Bnip3 1.13	Casp3 -1.18	Casp8 -1.42	Npc1 -1.00
C	Cdkn1b 1.28	Cdkn2a -7.30 A	Cln3 1.08	Ctsb 1.06	Ctsd -1.05	Ctss 1.37	Cxcr4 -2.58	Dapk1 1.61	Dram2 -1.38	Eif2ak3 1.02	Eif4g1 1.02	Esr1 -1.40
D	Fadd 1.29	Fas 1.01	Gaa 1.31	Gabarap 1.13	Gabarapl2 -1.65	Hdac1 -1.07	Hdac6 -1.41	Hgs 1.25	Hsp90aa1 -1.14	Htt -1.06	Ifng -1.55 A	Igf1 -1.43
E	Ins2 1.87 B	Irgm -1.26	Lamp1 1.03	Map1lc3a 1.69	Map1lc3b -1.04	Mapk14 -1.05	Mapk8 1.06	Mapt 1.32	Mtor -1.06	Nfkb1 1.16	Park2 -1.25	Park7 -1.33
F	Pik3c3 1.01	Pik3cg -1.52	Pik3r4 -1.11	Pim2 1.45	Pink1 1.53	Prkaa1 1.16	Psen1 -1.02	Pten -1.05	Rab24 1.13	Rb1 1.15	Rb1cc1 -1.22	RGD1359310 -1.27
G	Rgs19 -1.19	Rps6kb1 1.14	Snca -1.26	Sqstm1 1.97	Tgfb1 -1.09	Tgm2 1.09	Tm9sf1 1.06	Tnf 1.08	Tnfsf10 1.10	Tp53 1.10	Ulk1 -1.17	Wipi1 -1.01

B

Figure 14: Expression of autophagy-related genes in hearts of adenine-diet and control rats. **A**: heat map and **B**: array layout of expression of ageing-related genes in PCR array. Genes showing > 2-fold decrease in expression in the adenine group are circled in green, those showing > 2-fold increase in expression are circled in red (n = 5).

3.4.2 The effect of uraemia on ageing-related gene transcription

RNA was purified from snap-frozen cardiac tissues of the same adenine diet and control diet rats used in the autophagy array, reverse transcribed, and real-time PCR performed using a commercially available ageing-gene array. Fold-change in gene expression between groups was calculated using the 2^(-ΔΔCt) method (Figure 15).

Gene expression differed much more in the ageing than autophagy array, with 9 genes expressed more than threefold less in cardiac tissue from adenine-diet rats: *Bub1b (*-12.82 fold, p = 0.002584), *C3ar1* (-3.23 fold, p = 0.007384), *C5ar1* (-3.29 fold, p = 0.004562), *Ccr*1 (-3.23 fold), *Clu (-3.65 fold, p = 0.000281)*, *Col1a1* (-6.23 fold, p = 0.000281), *Gfap* (-3.6 fold, p = 0.002482), *Lmnb2* (-3.31 fold, p = 0.000829) and *Tlr4 (*-3.55 fold, p = 0.000226). *S100a8* and *S100a9* were expressed more than threefold more in cardiac tissue from adenine-diet rats than in that from control-diet animals (3.41 and 3.99 fold respectively, p = 0.004719 and 0.001880).

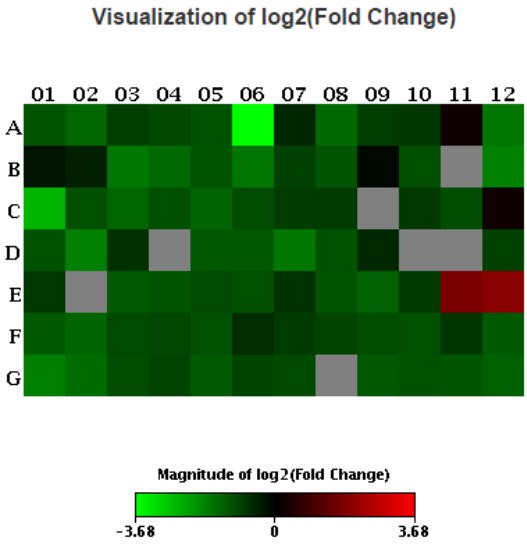

A

Layout	01	02	03	04	05	06	07	08	09	10	11	12
A	Angel2 -2.32	Anxa3 -2.80	Anxa5 -1.87	Arid1a -2.04	Arl6ip6 -2.26	Bub1b -12.82	C1qa -1.45	C1qb -2.81	C1qc -1.86	C1s -1.72	C3 1.18	C3ar1 -3.23
B	C4a -1.20	C4b -1.37	C5ar1 -3.29	Calb1 -2.86	Casp1 -2.32	Ccr1 -3.23	Cd14 -1.90	Cd163 -2.35	Cdkn1c -1.09	Cfh -2.23	Cfhr1 -1.39 C	Clu -3.65
C	Col1a1 -6.23	Cx3cl1 -2.22	Cxcl16 -2.75	Elavl1 -2.23	Eml1 -2.69	Ep300 -2.14	Fbxl16 -1.83	Fcer1g -1.82	Fcgbp -1.39 C	Fcgr1a -1.74	Fcgr2a -2.15	Fcgr2b 1.17
D	Foxo1 -2.27	Gfap -3.60	Hsf1 -1.60	Jakmip3 -1.39 C	Lmna -2.42	Lmnb1 -2.41	Lmnb2 -3.31	LOC100362548 -2.26	Lsm5 -1.49	Ltf -1.39 C	Lyzl1 -1.39 C	Mbp -1.90
E	Mrpl43 -1.76	Ndufb11 -1.39 C	Panx1 -2.48	Pdcd6 -2.33	Phf3 -2.11	Polrmt -2.24	Pot1 -1.65	Rap1a -2.36	RGD1564788 -2.69	Rnf144b -1.77	S100a8 3.41	S100a9 3.99
F	Scn2b -2.43	Sirt3 -2.73	Sirt6 -2.09	Smad2 -2.01	Snap23 -2.23	Terf1 -1.54	Terf2 -1.81	Tfam -1.96	Tfb1m -2.14	Tfb2m -2.22	Tinf2 -1.67	Tlr2 -2.39
G	Tlr4 -3.55	Tmem135 -2.94	Tmem33 -2.15	Tollip -1.92	Tpp1 -2.44	Txnip -1.97	Vps13c -2.11	Vwa5a -1.39 C	Zbtb10 -2.40	Zfp9 -2.28	Zfr -2.35	Zmpste24 -2.60

B

Figure 15: Expression of ageing-related genes in hearts of adenine-diet and control rats. **A**: heat map and **B**: array layout of expression of ageing-related genes in PCR array. Genes showing > 3-fold decrease in expression in the adenine group are circled in green, those showing > 3-fold increase in expression are circled in red (n = 5).

3.4.3 Discussion

Only one autophagy-related gene was expressed more than twofold less in cardiac tissue from adenine-diet rats than in those from control-diet animals. This is consistent with the received wisdom that changes in autophagy take place at post-translational level[108]. Nonetheless, those that were altered are of interest.

Cxcr4 (-2.58 fold, p = 0.019958 by Student's t-test) encodes for the chemokine receptor CXCR4, which is expressed in cardiac myocytes and fibroblasts[136]. Mice heterozygous for CXCR4 (*Cxcr4*$^{+/-}$) have significantly reduced CXCR4 cellular surface expression than wild-type mice. *Cxcr4*$^{+/-}$ mice demonstrate reduced infarct size at 4 weeks after experimental myocardial infarction (MI) compared with controls. This is associated with altered inflammatory cell recruitment, decreased neutrophil content, and delayed monocyte infiltration. However, basal coronary blood flow and its recovery after MI are impaired, paralleled by reduced angiogenesis, myocardial vessel density, and endothelial cell count. The authors of this study conclude that the *Cxcr4*$^{+/-}$ mouse can be considered as a model for congenitally impaired vascularization and adaptation to hypoxia[137]. The decreased expression of *Cxcr4* in uraemic rat hearts suggests a similar adaptation to conditions of chronic ischaemia seen in uraemic cardiomyopathy[138].

Only *Bcl2l1* was expressed more than twofold (2.67 fold, p = 0.0005) more in cardiac tissue from adenine-diet rats than in that from control-diet animals. *Bcl2l1* encodes for two proteins, Bcl-xL and Bcl-xS[139]. *Bcl2l1*/Bcl-xL has been proposed as a regulator of mitophagy,

the selective removal of damaged mitochondria by autophagy[139]. Under normoxic conditions *Bcl2l1*/Bcl-xL suppresses autophagy, whereas in conditions of hypoxia it induces it (as mentioned in Chapter 1, 1.4.1, page 27), increasing mitochondrial turnover and decreasing apoptosis[139]. From this it might be inferred that the upregulation of *Bcl2l1* in the uraemic heart acts to increase mitochondrial turnover and thus generate energy and prevent apoptosis under hypoxic conditions. This idea is consistent with the findings of increased autophagy in uraemia demonstrated by immunoblot, and also the increased response to ischaemic pre-conditioning demonstrated by other investigators[86].

Gene expression in adenine-diet and control-diet rat hearts differed much more on the ageing array (it should be noted that neither array used was tissue-specific, therefore whilst clearly expressed in cardiac tissue, not all of these genes have a clearly defined role in the heart, pertinent to this thesis or otherwise).

Lmnb2 is particularly interesting, as it encodes for lamin B2, a protein involved in the formation of the nuclear envelope[140]. Lamin A, a nuclear envelope protein encoded by *Lmna* (itself expressed – 2.42 fold in adenine-diet rat cardiac tissue, p = 0.004299) , is the protein truncated in Hutchinson-Gilford progeria[141], a condition which demonstrates striking similarities to the uraemic phenotype, especially with regards to the cardiovascular system: Hutchinson-Gilford progeria sufferers die at a mean age of 14, primarily of stroke and MI, and demonstrate a similar pattern of accelerated arteriosclerosis and atherosclerosis to CKD sufferers[13].

Bub1b encodes for BubR1, a spindle assembly checkpoint protein which acts to maintain genetic stability by ensuring faithful segregation of replicating chromosomes[142]. Mutant mice with low levels of BubR1 demonstrate a variety of progeroid features, including poor wound healing[142], which is also exhibited by patients with end stage kidney disease[143].

S100A8 (calgranulin A or migration inhibitory factor-related protein 8, MRP8) and its binding partner S100A9 (calgranulin B or MRP-14) are members of the S100 calcium-binding family of proteins, which are increased in a number of inflammatory and autoimmune states[144]. S100A8/A9 immunoreactivity has been demonstrated in atherosclerotic plaques in humans[145], especially in rupture-prone lesions compared to stable ones[146]. Plasma levels of S100A9 have been demonstrated to predict the risk of future nonfatal MI, nonfatal stroke, and cardiovascular death in apparently healthy women[147]. S100A8/A9 have been shown to be early markers for detection of acute coronary syndrome (ACS)[148], and the risk of a recurrent cardiovascular event was increased with each increasing quartile of S100A8/A9 in the PROVE IT-TIMI 22 trial[149]. Increased expression of *S100a8* and *S100a9* in the uraemic rat heart therefore suggests a pro-atherosclerotic state.

These findings, whilst not necessarily relating to the *Cdkn2a/*p16^{Ink4a}/p14^{ARF}/p53 senescence pathway, do describe a progeroid, pro-ischaemic state in the uraemic heart, in which autophagy is perhaps upregulated as a compensatory, protective mechanism.

3.5: Histology for autophagy activity: immunohistochemistry and fluorescence microscopy

3.5.1 Autophagy activity in young and old mice

Attempts were made to use immunohistochemistry to assess autophagy in tissues, by staining for LC3. It was immediately apparent that this had several drawbacks. The same antibody detects both LC3I and II, and whilst this is the basis of immunoblotting for autophagy, it makes it extremely difficult to assess autophagy activity in tissues. Theoretically, an increase in LC3 'punctae' compared to diffuse, cytoplasmic staining is indicative of an increase in autophagy. This is profoundly difficult to judge and becomes somewhat arbitrary. Additionally, it was found to be difficult to detect LC3B in tissues, but an overly intense stain was achieved with LC3A.

2-month and 24 month-old mice were sacrificed after either 24 h starvation or having been fed a normal diet until death. All were given chloroquine 10mg/kg IP 4 h prior to sacrifice. Cardiac tissues were harvested and snap frozen. Sections were stained for LC3B and H&E (Figure 16).

Immunohistochemical staining for LC3B in non-fasted and fasted young and elderly mouse hearts did suggest that, whilst the absolute extent of autophagy in both states was greater in

younger mice, the increase in LC3B punctae between the non-fasted and fasted states was actually significantly greater in elderly mice, suggesting a greater upregulation of autophagy.

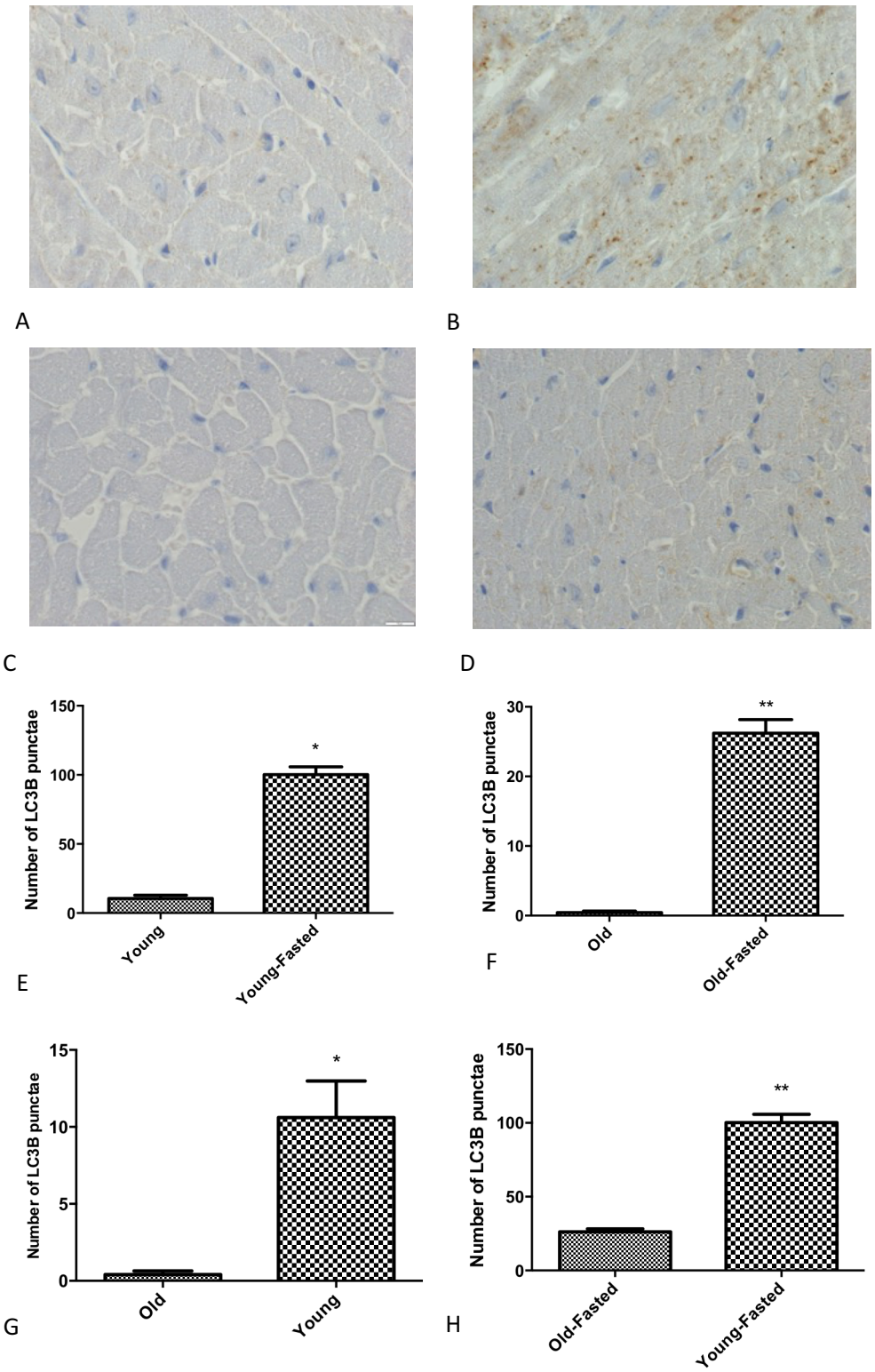

Figure 16: Autophagic activity in cardiac tissues in non-fasted and fasted young and elderly mice. **A**: Section of cardiac tissue from non-fasted, young mouse. **B**: Section of cardiac tissue from fasted, young mouse. **C**: Section of cardiac tissue from non-fasted, elderly mouse**. D**: Section of cardiac tissue from fasted, elderly mouse. **E**: Graph showing mean number of LC3B punctae on 5 randomly selected fields from sections of cardiac tissue of young, non-fasted and young, fasted mice (∗ denotes p value of 0.012 by Mann-Whitney U test). **F**: Graph showing mean number of LC3B punctae on 5 randomly selected fields from sections of cardiac tissue from elderly, non-fasted and elderly, fasted mice (∗∗ denotes p value of 0.008 by Mann Whitney U test). **G**: Graph showing mean number of LC3B punctae on 5 randomly selected fields from sections of cardiac tissue from non-fasted elderly and young mice (∗ denotes p value of 0.011 by Mann Whitney U test). **H**: Graph showing mean number of LC3B punctae on 5 randomly selected fields from sections of cardiac tissue from fasted elderly and young mice (∗∗ denotes p value of 0.008 by Mann Whitney U test).

3.5.2 The effect of uraemia on cardiac autophagy in GFP-LC3 mice

Attempts were made to assay autophagy in the uraemic heart using GFP-LC3 mice. These were fed either an adenine or control diet, fasted for 24 h, and half given 10 mg/kg chloroquine i.p. 4 hours before being sacrificed. Tissues were sectioned, stained with DAPI, and viewed under a fluorescent microscope. Punctae fluorescing under a GFP but not RFP filter set were identified, confirming them as GFP-LC3 rather than autofluorescent granules[150]. 5 fields were randomly selected from sections and the number of punctae on each field counted by a blinded assessor (Figure 17).

Interestingly, whilst the number of GFP-LC3 punctae appeared to be greater in fasted adenine-diet mouse hearts than control-diet mouse hearts, this effect was cancelled out by the addition of chloroquine. This could be interpreted as showing that adenine-diet mice actually exhibited *less* autophagy, the greater number of GFP-LC3 punctae seen in mice who had not received chloroquine being the result of inhibition of autolysosome breakdown, rather than increased autophagosome formation. However, it is somewhat odd that LC3-GFP numbers appear to be less (albeit insignificantly) in the chloroquine-treated animals. This might suggest an error in chloroquine administration or malabsorption. The experiment needs to be repeated with greater numbers of animals.

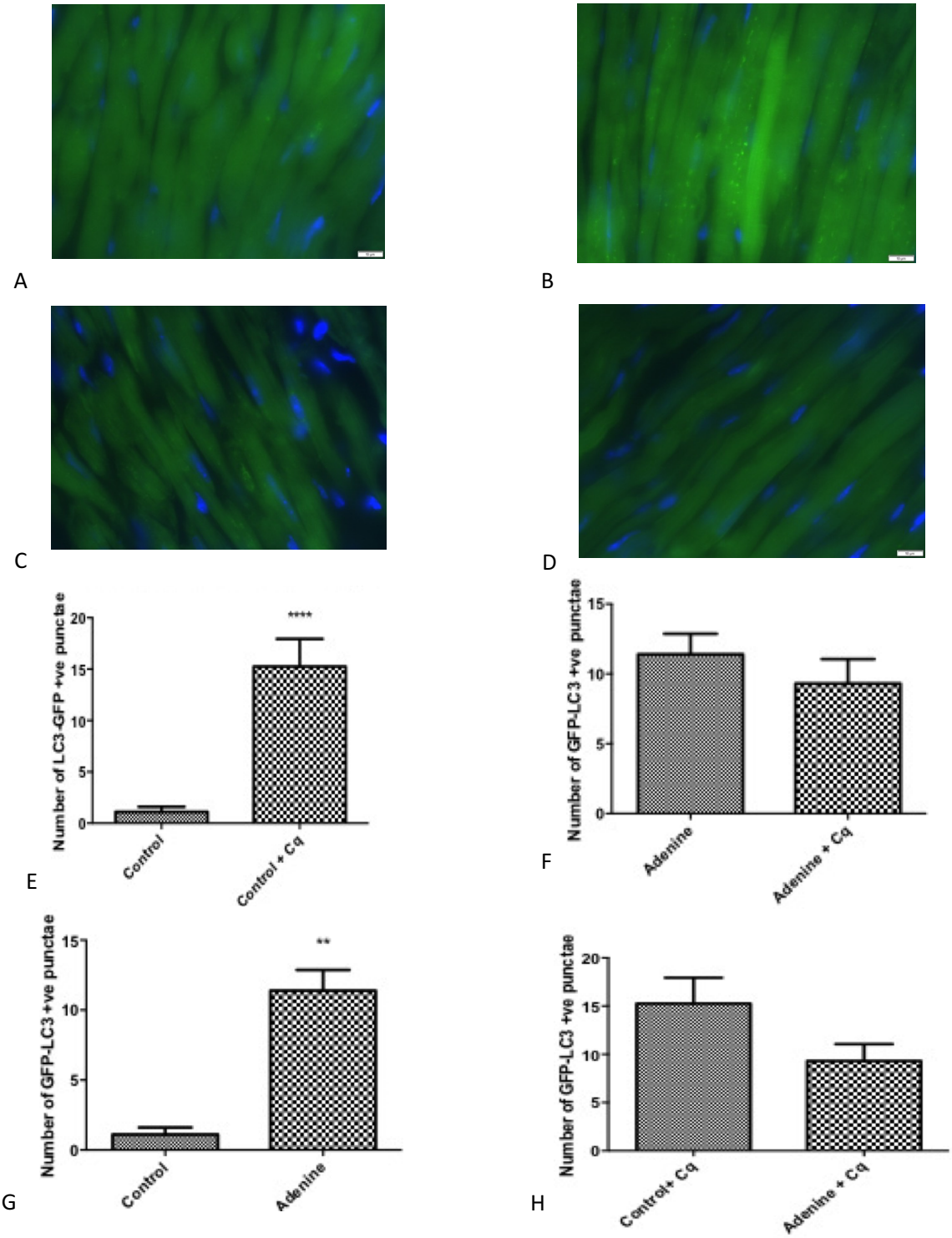

Figure 17: Fluorescence microscopy for autophagy activity in cardiac tissues of adenine-diet and control GFP-LC3 mice. **A**: Section of cardiac tissue from a GFP-LC3 control diet mouse, fasted for 24 h prior to sacrifice. **B**: Section of cardiac tissue from a GFP-LC3 control diet mouse, fasted for 24 h and given chloroquine prior to sacrifice. **C**: Section of cardiac tissue from GFP-LC3 adenine diet mouse, fasted for 24 h prior to sacrifice. **D**: Section of cardiac tissue from GFP-LC3 adenine diet mouse, fasted for 24 h and given chloroquine prior to sacrifice. **E**: Graph showing mean number of LC3-GFP punctae per field on sections of cardiac tissue from control diet, fasted, GFP-LC3 mice with and without chloroquine (•••• denotes p value of < 0.0001 by Mann Whitney U test, n = 2 and 3). **F**: Graph showing mean number of LC3-GFP punctae per field on sections of cardiac tissue from adenine diet, fasted, GFP-LC3 mice with and without chloroquine. **G**: Graph showing mean number of GFP-LC3 punctae per fluorescent microscopy field on sections of fasted, control and adenine diet GFP-LC3 mice (** denotes p value of 0.002, n = 2 and 1). **H**: Graph showing mean number of GFP-LC3 punctae per field on sections of fasted, control and adenine diet GFP-LC3 mice with chloroquine.

3.5.3 Discussion

Immunohistochemical staining for LC3B in young and elderly non-fasted and fasted mouse hearts (albeit very limited) suggests that whilst basal and reactive autophagy are decreased in absolute terms in the elderly, the relative increase in autophagy under stressful conditions is, in fact, greater in the elderly. This is consistent with the findings of Sengstock *et al.* of increasing patient age being associated with increased autophagy in cardiac tissue from patients undergoing heart surgery[151]. Additionally, this may have parallels in uraemia: it has previously been demonstrated that uraemic hearts are more susceptible to infarction than non-uraemic ones, but that the myocardial protective effect of ischaemic preconditioning (an example of hormesis, a possibly autophagy-dependent phenomenon) is greater in uraemia[86]. Thus the finding of increased autophagy in cardiac tissues in starved, uraemic rats does not discount an aged phenotype: in fact it might support it.

Enzymatic staining for β-galactosidase

Staining for β-galactosidase in the hearts and livers of control and uraemic rats was unsuccessful. It is well established that senescent cells are, in actual fact, quite scarce in tissues[18], and it is quite possible that they are effectively undetectable in only two-month old mice, uraemic or otherwise. It may have been better to repeat the experiment in comparatively older animals, in which a greater degree of senescence could be detected even in health.

Chapter 4: General Discussion

4.1 Introduction

The aim of this thesis was to assess the effect of uraemia on autophagy and senescence in the heart, the nature of their relationship, and how this contributes to the pathologically aged cardiac uraemic phenotype, using *in vitro* and *in vivo* models of uraemia.

IS appeared to induce autophagy in cardiac myocytes *in vitro*, and autophagy seemed to be upregulated *in vivo* in cardiac tissues in an adenine-diet rodent model of uraemia (though this did not achieve statistical significance). A marker of autophagy activity was significantly increased in hepatic tissues in a 5/6 nephrectomy rodent model of uraemia. Although the transcription of autophagy-related genes in the hearts of uraemic rats did not differ greatly from that in healthy animals, the genes that were more or less expressed suggest a 'pro-autophagy' state at a transcriptional level in the uraemic heart, though this is likely reactionary rather than constitutive. Whilst differences in senescence-related protein expression in cardiac tissues were not seen between uraemic and healthy rats, the pattern of expression on the ageing-related gene array seen described a progeroid, pro-atherosclerotic, pro-ischaemic state in the uraemic heart, in which autophagy may be upregulated by way of a compensatory response. Clear parallels can be drawn between this and the physiology and behaviour of the aged heart. Additionally, it has been reconfirmed that nutritional status can influence autophagy, and that this and other potential confounders needs to be considered when designing *in vivo* experiments assaying autophagy in a disease process.

4.2 The effect of uraemia on autophagy

4.2.1 Immunoblotting

IS (a recognised uraemic toxin[131]) appeared to stimulate autophagy in H9c2 cells with the greatest difference versus control noticeable at 48 h with 25 μg/mL of IS. Interestingly this is approximately the mean concentration found in the serum of patients on thrice weekly haemodialysis[134]. IS is known to be toxic to cells: amongst other effects it induces oxidative stress[152], a known trigger for autophagy[153]. It is thus tempting to speculate that uraemia, via the actions of 'uraemic toxins' such as IS, is a stressor that induces survival responses (such as autophagy) in cardiac cells. The *in vitro* model is particularly useful here, as it controls for potential confounders such as poor nutritional status driving autophagy, though it should be noted that these experiments involved limited numbers and would need to be repeated in order to achieve statistical significance.

It should be noted that LC3BII detection did seem to decline beyond 50 μg/mL of IS, though remained above that seen in control cells. It might be postulated that higher doses of uraemic toxins actually have an inhibitory effect on autophagy, though these would not be representative of IS concentrations in patients with CKD, and therefore of little translational interest. Additionally, it must be taken into account that 24 h and 48 h of exposure to IS represents an acute insult, therefore this may not be representative of the chronic uraemic state. It is quite possible that autophagy is initially upregulated then either remains steady or declines. Furthermore, evidence that autophagosome formation and destruction is

upregulated, even if corroborated by evidence of p62 destruction, does not confirm that all functions of autophagy are increased to successful completion.

Two rodent models of uraemia were used: adenine-diet and 5/6 nephrectomy. Autophagy activity was seen to be increased (though not significantly) in the hearts of adenine-diet rats as evidenced by increased detection of LC3II and beclin-1 on immunoblot. Additionally, autophagy activity was significantly increased in the livers of 5/6 nephrectomy rats (as seen in section 3.3.2).

Animals on the adenine-diet tend to eat less than animals on a normal, control feed (perhaps finding the diet less palatable), and uraemic animals of both types tend to weigh less than controls[123]. Nutritional state is known to affect autophagy activation via mTOR and AMPK signalling pathways[48], and is thus a potential confounding factor, therefore all animals were fasted for 24 h prior to tissue retrieval in an effort to standardise the degree of influence acute nutritional state had on autophagy. This perhaps meant assessing the differences in the acute, 'induced' autophagic response to acute starvation between control and uraemic animals, as opposed to background, 'basal' autophagy[50]. In order to assess the effect of uraemia on basal autophagy a way might need to be found to control for nutritional deficiencies without introducing an acute stressor. This is very hard to achieve given that anorexia and cachexia are features of many chronic disease states. However, human studies have shown that hypoxia-induced upregulation of cardiac autophagy may be greater in older subjects[151], as was starvation-induced upregulation of autophagy in my immunohistochemical stains of fasted, elderly mouse hearts. This increased upregulation of autophagy in the face of cellular

stress could explain, in part, the findings of Byrne *et al.* that, whilst infarct size is increased in a model of myocardial infarction in uraemic animals, ischaemic preconditioning, a technique that may confer protection via autophagy induction, is actually more effective in uraemic animals than healthy controls[86].

Conversely, it is also possible that fasting the animals for 24 h did not adequately correct for the chronically nutritionally-deplete state of the uraemic animals of both models, thus the control animal's response was not sufficiently induced to offer an accurate comparison. Some might suggest that the experiment needs to be repeated without chloroquine in order to determine whether successful lysosomisation takes place following upregulated autophagy i.e. completed flux takes place[108]. It is quite possible that autophagy is upregulated but is not completed and is therefore dysfunctional.

Finally, it is possible that both models of uraemia reflect acute kidney injury more than CKD. This is likely true more of the adenine diet model, in which animals are strikingly uraemic, but for a relatively short length of time, and demonstrate fewer of the morphological and physiological features of CKD[123]. It is thus possible that acute uraemia may induce autophagy, but in longstanding uraemia autophagy may plateau or decline. This would be in keeping with the finding of Chen *et al.* of decreased autophagy activity in circulating leucocytes in patients with end stage kidney disease[89].

Sample sizes were small due to the labour intensiveness and complexity of immunoblotting for autophagy (in particular), and greater numbers would be required to determine statistical significance in some cases.

Work using fluorescent microscopy in GFP-LC3 mice seemed to provide a contradictory result to my immunoblotting, in that less GFP-LC3 punctae were seen in the cardiac tissues of fasted adenine-diet mice than in controls. However, the fact that chloroquine administration decreased the number of GFP-LC3 punctae is very difficult to explain.

4.2.2 PCR

There is some disagreement in the field of autophagy-related research as to whether changes in autophagy activity are mirrored at a transcriptional level[108]. Nonetheless, the genetics of autophagy has been partially characterised, and a significant number of genes encoding proteins involved in the machinery and modulation of autophagy have been identified[46]. Therefore, changes in the expression of autophagy-related genes with different conditions (even if not corresponding to changes in autophagic flux) are of interest.

Whilst changes in gene expression were neither widespread nor dramatic, the genes which were expressed differently in adenine-diet rat cardiac tissue did allude to a 'pro-autophagy' state. An increase in the expression of *Bcl2l1* would, in turn, result in an increased expression of Bcl-xl, which in conditions of hypoxia and starvation actually stimulates autophagy and in particular mitophagy, increasing mitochondrial turnover, generating energy and preventing apoptosis[139]. A decrease in the expression of *Cxcr4* may reflect an adaptation to limit infarction in a chronically ischaemic, hypoxic, uraemic myocardium[137], in which autophagy is upregulated as a compensatory response. This parallels the increase in autophagy suggested

by my immunoblotting work. I would argue that the fact that genes encoding key proteins involved in the autophagy machinery were not upregulated reconfirms that autophagy modulation is largely post-translational, and that the increase in autophagy I detected was as a response to stress rather than a programmed cause of uraemic cardiomyopathy.

It should be noted that the animals in this experiment were not fasted, thus it would be interesting to repeat it in fasted conditions to determine whether there is a change in *Bcl2l1* expression. Again, this would further elucidate whether uraemia affects basal and inducible autophagy in different ways. Furthermore, a gene array is, in essence, a 'fishing exercise', therefore evidence of changes in gene expression, whilst interesting, need to be corroborated by changes at a translational and post-translational level. An obvious next step would be to look at the expression of the proteins encoded by these genes in cardiac tissues in uraemic and control animals, and those others they are linked to in the regulation of autophagy.

Overall these findings are consistent with previous experimental evidence that suggests that changes in autophagy activity are not widely reflected at a transcriptional level[108]. However, the differences in transcription seen here do hint at some interesting differences at a genetic level between control and uraemic animals, albeit without proof of translational differences, and suggest the *Bcl2l1* locus as areas of ongoing investigation into the effect of uraemia on autophagy in the uraemic heart.

4.3 The effect of uraemia on senescence

4.3.1 Immunoblotting

Initial experiments were performed to determine how markers of senescence were expressed in elderly (and by expectation senescent) rodents. The intention was to characterise an 'elderly' pattern of protein expression, against which that in uraemia could be compared. Elderly (twenty-four month-old) mice were used for these experiments as they were considerably cheaper than rats, and markers of both autophagy and senescence are highly conserved across species[50,2]. p53 and $p16^{Ink4a}$ were chosen as markers of senescence for immunoblot studies due to their consistent expression with ageing in most tissues and species[22]. Unfortunately, it was very difficult to find an effective antibody to $p16^{Ink4a}$ (as has been previously mentioned in the literature[18]) and it was only towards the end of my experimentation that I was reliably able to detect it. The expression of p53 and $p16^{Ink4a}$ was significantly increased in the heart of 24-month compared to 2-month old mice (in fact these markers of senescence were barely detectable in the latter). These findings established that expression of p53 and $p16^{Ink4a}$ correlates with ageing in rodent tissues, and these (certainly the former) can be reliably measured in *in vivo* models.

p53 expression did not differ significantly in cardiac tissue from adenine diet and control rats, nor in hepatic tissue from 5/6 nephrectomy and control rats. Experimental and control animals were the same age; therefore, this was not a confounder. Thus a corollary of my previous statement regarding the utility of p53 expression in predicting advanced age would

be that uraemia does not increase senescence in cardiac tissues in rats. However, p53 expression is only one measure of senescence, thus this cannot be seen as definitive evidence that senescence is not increased in uraemia. Additionally, as has been previously discussed, it remains unclear as to whether senescence has a causative role in ageing, or is merely an associated phenomenon.

Adijiang *et al.* proposed to have demonstrated that that uraemic toxins cause increased senescence in rat aortas *in vivo*, as detected by an increase in SA-β-GAL staining, and p53 and $p16^{Ink4a}$ expression[94]. This group employed an unusual model in which they administered IS to hypertensive rats, which seems a fairly unrepresentative model of uraemia and difficult to compare to those used by our group.

4.3.2 PCR

Differences in gene expression were greater and more numerous between adenine-diet and control rat hearts using the ageing compared to autophagy array. The expression pattern in the adenine-diet rat hearts seemed to reflect a progeroid, pro-ischaemic, pro-atherosclerotic state in the uraemic heart. The finding of downregulation of *Bub1b* and *Lmnb2* invites comparison with known models of BubR1 deficiency (mutant mice) and lamin abnormalities (Hutchinson-Gilford progeria), both of which demonstrate an accelerated ageing phenotype with striking similarities to that seen in uraemia. An increase in *S100a8/a9* may be taken to reflect the pro-atherosclerotic state of the uraemic heart and vasculature.

This array was not specific to senescence *per se*, nor did it demonstrate any changes in the *Cdkn2a*/p16^{Ink4a}/p14^{ARF}/p53 pathway, but it perhaps provides even more useful information pertaining to the general state of ageing in the uraemic heart. Whilst, once again, this information needs to be corroborated by translational and post-translational work, the cumulative evidence points to a state of accelerated ageing and ischaemia in the uraemic heart, in which survival mechanisms such as autophagy are upregulated by way of compensation. The findings of the ageing array also provide novel and numerous future avenues of investigation.

4.4 Summary

The work presented here has demonstrated several possible methods of assaying autophagy and senescence, the former *in vitro* and *in vivo*, and the latter *in vivo*. Both processes are notoriously difficult to detect and measure, especially in the context of an ill-defined syndrome such as uraemia.

Evidence has been provided to suggest that autophagy is altered in uraemia, with a possible upregulation of autophagy in cardiac cells exposed to a uraemic toxin, and in cardiac and hepatic tissues from fasted, uraemic animals. Additionally, there were differences (albeit expectedly few) in the transcription of autophagy-related genes in non-fasted uraemic hearts that may be interpreted to demonstrate an upregulation of autophagy at a transcriptional level in response to cellular stress. Whilst the detection of the senescence marker p53 by immunoblot did not differ in uraemic and control rat hearts the wider expression of ageing-

related genes did, describing a progeroid, ischaemic environment in which it is conceivable that autophagy is upregulated as a compensatory survival mechanism in order to prevent apoptosis and necrosis.

It seems logical that autophagy should be upregulated in the uraemic heart given that it is known to be increased in conditions of stress, e.g. myocardial ischaemia[130] and oxidative stress[154]. Studies which have purported to show a decrease in autophagy in uraemia in humans[89] are inherently flawed as they are unable to accurately measure autophagic flux: it is not possible (nor desirable) to block lysosomisation *in vivo* in human subjects.

A state of increased autophagy does not necessarily exclude a progeroid one. Whilst it has become dogma that autophagy declines with cardiac ageing, based on indirect evidence provided by lipofuscin and ROS studies in the aged heart[103,154,155,156] , there is much published material that contradicts this[151,157]. Of particular note is the study by Boyle *et al.* of ageing-related cardiomyopathy in mice[158]. Serial echocardiography was performed on the same cohort of mice every 3 months, demonstrating an increase in left ventricular hypertrophy (LVH) and fibrosis. Electron microscopy of left ventricular tissue showed an increase in autophagic vacuoles in cardiac myocytes in the older mice, with increased expression of beclin-1 and an increased LC3II to I ratio. Markers of apoptosis were increased in the elderly hearts[158]. The authors conclude that the increase in autophagy in the ageing heart is a protective mechanism upregulated in attempt to prevent further apoptosis[158]. I would argue that this is strikingly analogous to the situation in the uraemic heart.

Moreover, uncertainty remains as to whether an increase in autophagy is necessarily cardio-protective: excessive autophagy may contribute to doxorubicin-mediated cardiac injury[159]. Thus, regardless of its correlation with an ageing phenotype, it still remains to be elucidated whether an increase or decrease in autophagy in ageing (or uraemia) is causative, reactive, or circumstantial.

During the course of my investigations I have replicated other authors' work with regards to the effect of glucose deprivation and, more pertinently, rapamycin on autophagy in cardiac myocytes. Whilst the latter has been shown to prevent the development of uraemic cardiomyopathy in rodents[90] no such studies have been performed in humans, and it would be interesting to assess transplant patients taking rapamycin with echocardiography to see whether this was the case.

A more thorough investigation of the influence of uraemia on autophagy would be to repeat all experiments in adenine-diet LC3-GFP mice in both non-fasted and fasted states, with and without intraperitoneal chloroquine. This would assess both the extent of induction and successful completion of both basal and reactive/inducible autophagy. Based on my experiments I would pursue immunoblotting and fluorescence microscopy for LC3 as the best measures of autophagy (LC3-GFP transgenic animals offer another means of immunoblotting for autophagy, the amount of free GFP fragment indicating the amount of completed autophagic flux[108]). Senescence is best assessed by immunoblotting for p53 and (with a good antibody) $p16^{Ink4a}$, both of which could simultaneously be assessed alongside markers of autophagy. I suspect that performing experiments in slightly older animals might offer a

better chance of successful β-galactosidase detection and comparison between groups. The plethora of information provided by the ageing-related PCR array has provided a number of alternative pathways of ageing to investigate. Experiments to investigate the relationship between autophagy and senescence might be to inhibit (for instance using 3-methyladenine, 3-MA) or induce (using rapamycin) autophagy, then assess the impact this has on senescence. This could be done *in vitro* or *in vivo*. Phenotypic correlation could be provided by serial echocardiography.

It should be emphasised that numbers were small in these experiments and repetition would allow for more robust conclusions to be made.

Translational experimentation is very difficult. One group of patients already taking a known autophagy-inducer are renal transplant patients receiving treatment with rapamycin. These patients could be assessed physiologically for evidence of a decrease in phenotypic markers of cardiac ageing (for instance a decrease in cardiac hypertrophy on echocardiogram), alongside molecular evidence of increased autophagy and senescence. Additional methods of manipulating autophagy would be experiments with relative calorie deprivation, intermittent fasting or exercise in patients with chronic kidney disease.

There is an increasing body of evidence (of which this thesis may serve some small part) that ageing-related molecular pathways are altered in uraemia. This is a very new and under-explored field of research, but in time may lead to novel therapies targeting these pathways. In the meantime, clinicians should, perhaps, appreciate more that patients with advanced

kidney disease are physiologically much akin to the elderly (regardless of the molecular mechanisms underpinning this), and measures such as frailty scores and fall risks might perhaps be better predictors of outcomes than investigations employed in non-affected persons, interventions such as exercise may be of great benefit, and a general approach that acknowledges a degree of progeria likely to prove most beneficial.

References

1. Kooman, J. P. *et al.* Out of control: Accelerated aging in uremia. *Nephrol. Dial. Transplant.* **28,** 48–54 (2013).

2. López-Otín, C. *et al*. The hallmarks of aging. *Cell* **153,** (2013).

3. Koopman, J. J. *et al.* Senescence rates in patients with end-stage renal disease: a critical appraisal of the Gompertz model. *Aging Cell* **10,** 233–238 (2011).

4. Foley, R. N. *et al.* Epidemiology of cardiovascular disease in chronic renal disease. *J. Am. Soc. Nephrol.* **9,** S16–S23 (1998).

5. Amann, K. & Ritz, E. Cardiovascular abnormalities in ageing and in uraemia--only analogy or shared pathomechanisms? *Nephrol. Dial. Transplant* **13 Suppl 7,** 6–11 (1998).

6. Kato, S. *et al.* Aspects of immune dysfunction in end-stage renal disease. *Clin. J. Am. Soc. Nephrol.* **3,** 1526–1533 (2008).

7. Betjes, M. G. H. *et al*. Loss of renal function causes premature aging of the immune system. *Blood Purif.* **36,** 173–178 (2014).

8. Fried, L. P. *et al.* Frailty in older adults: evidence for a phenotype. *J. Gerontol. A. Biol. Sci. Med. Sci.* **56,** M146–M156 (2001).

9. Johansen, K. L. *et al*. Significance of frailty among dialysis patients. *J. Am. Soc. Nephrol.* **18,** 2960–2967 (2007).

10. Kurella Tamura, M. & Yaffe, K. Dementia and cognitive impairment in ESRD: diagnostic and therapeutic strategies. *Kidney Int.* **79,** 14–22 (2011).

11. Van Walraven, C. *et al*. Survival Trends in ESRD Patients Compared With the General

Population in the United States. *Am. J. Kidney Dis.* (2013).

12. White, W. E. *et al.* Aging and uremia: Is there cellular and molecular crossover? *World J. Nephrol.* **4,** 19 (2015).

13. Kooman, J. P. *et al*. Chronic kidney disease and premature ageing. *Nat. Rev. Nephrol.* **10,** 732–42 (2014).

14. Campisi, J. & d'Adda di Fagagna, F. Cellular senescence: when bad things happen to good cells. *Nat. Rev. Mol. Cell Biol.* **8,** 729–740 (2007).

15. Hayflick, L. & Moorehead, P. S. The serial cultivation of human diploid cell strains. *Exp. Cell Res.* **25,** 585–621 (1961).

16. Harley, C. B. *et al*. Telomeres shorten during ageing of human fibroblasts. *Nature* **345,** 458–60 (1990).

17. Olovnikov, A. M. Telomeres, telomerase, and aging: origin of the theory. *Exp. Gerontol.* **31,** 443–448 (1996).

18. Childs, B. G. *et al*. Cellular senescence in aging and age-related disease: from mechanisms to therapy. *Nat. Med.* **21,** 1424–35 (2015).

19. Alcorta, D. A. *et al.* Involvement of the cyclin-dependent kinase inhibitor p16 (INK4a) in replicative senescence of normal human fibroblasts. *Proc. Natl. Acad. Sci. U. S. A.* **93,** 13742–7 (1996).

20. Takahashi, A. *et al.* Mitogenic signalling and the p16INK4a-Rb pathway cooperate to enforce irreversible cellular senescence. *Nat. Cell Biol.* **8,** 1291–1297 (2006).

21. Beauséjour, C. M. *et al.* Reversal of human cellular senescence: Roles of the p53 and p16 pathways. *EMBO J.* **22,** 4212–4222 (2003).

22. Krishnamurthy, J. *et al.* Ink4a/Arf expression is a biomarker of aging. *J. Clin. Invest.* **114,** 1299–1307 (2004).

23. Hayflick, L. The limited in vitro lifetime of human diploid cell strains. *Exp. Cell Res.* **37,** 614–636 (1965).

24. Dimri, G. P. *et al.* A biomarker that identifies senescent human cells in culture and in aging skin in vivo. *Proc. Natl. Acad. Sci. U. S. A.* **92,** 9363–7 (1995).

25. Kuilman, T. *et al*. The essence of senescence. *Genes and Development* **24,** 2463–2479 (2010).

26. Rodier, F. & Campisi, J. Four faces of cellular senescence. *Journal of Cell Biology* **192,** 547–556 (2011).

27. Blasco, M. A. *et al.* Telomere length, stem cells and aging. *Nat. Chem. Biol.* **3,** 640–649 (2007).

28. Armanios, M. *et al.* Short Telomeres are Sufficient to Cause the Degenerative Defects Associated with Aging. *Am. J. Hum. Genet.* **85,** 823–832 (2009).

29. Tomás-Loba, A. *et al.* Telomerase Reverse Transcriptase Delays Aging in Cancer-Resistant Mice. *Cell* **135,** 609–622 (2008).

30. Jaskelioff, M. *et al.* Telomerase reactivation reverses tissue degeneration in aged telomerase-deficient mice. *Nature* **469,** 102–106 (2011).

31. Bernardes de Jesus, B. *et al.* Telomerase gene therapy in adult and old mice delays aging and increases longevity without increasing cancer. *EMBO Mol. Med.* **4,** 691–704 (2012).

32. Boonekamp, J. J. *et al*. Telomere length behaves as biomarker of somatic redundancy

rather than biological age. *Aging Cell* **12,** 330–332 (2013).

33. Jeck, W. R. *et al.* Review: A meta-analysis of GWAS and age-associated diseases. *Aging Cell* **11,** 727–731 (2012).

34. Varela, I. *et al.* Accelerated ageing in mice deficient in Zmpste24 protease is linked to p53 signalling activation. *Nature* **437,** 564–568 (2005).

35. Matheu, A. *et al.* Delayed ageing through damage protection by the Arf/p53 pathway. *Nature* **448,** 375–379 (2007).

36. Begus-Nahrmann, Y. *et al.* p53 deletion impairs clearance of chromosomal-instable stem cells in aging telomere-dysfunctional mice. *Nat. Genet.* **41,** 1138–1143 (2009).

37. Koga, H. *et al*. Protein Homeostasis and Aging: the importance of exquisite quality control. *Ageing Res. Rev.* **10,** 205–215 (2012).

38. Powers, E. T. *et al*. Biological and chemical approaches to diseases of proteostasis deficiency. *Annu. Rev. Biochem.* **78,** 959–991 (2009).

39. Lee, I. H. *et al.* A role for the NAD-dependent deacetylase Sirt1 in the regulation of autophagy. *Proc. Natl. Acad. Sci. U. S. A.* **105,** 3374–3379 (2008).

40. Liu, G. *et al*. EGF signalling activates the ubiquitin proteasome system to modulate C. elegans lifespan. *EMBO J.* **30,** 2990–3003 (2011).

41. Deter, R. L. & De Duve, C. Influence of glucagon, an inducer of cellular autophagy, on some physical properties of rat liver lysosomes. *J. Cell Biol.* **33,** 437–449 (1967).

42. Glick, D. *et al.* Autophagy : cellular and molecular mechanisms. *J. Pathol.* **221,** 3–12 (2010).

43. Saftig, P. *et al*. LAMP-2. *Autophagy* **4,** 510–512 (2008).

44. Mizushima, N. & Klionsky, D. J. Protein turnover via autophagy: implications for metabolism. *Annu. Rev. Nutr.* **27,** 19–40 (2007).

45. Maiuri, M. C. *et al*. Self-eating and self-killing: crosstalk between autophagy and apoptosis. *Nat. Rev. Mol. Cell Biol.* **8,** 741–752 (2007).

46. Nakatogawa, H. *et al*. Dynamics and diversity in autophagy mechanisms: lessons from yeast. *Nat. Rev. Mol. Cell Biol.* **10,** 458–467 (2009).

47. Kroemer, G. *et al*. Autophagy and the Integrated Stress Response. *Molecular Cell* **40,** 280–293 (2010).

48. Green, D. R. & Levine, B. To be or not to be? How selective autophagy and cell death govern cell fate. *Cell* **157,** 65–75 (2014).

49. Axe, E. L. *et al.* Autophagosome formation from membrane compartments enriched in phosphatidylinositol 3-phosphate and dynamically connected to the endoplasmic reticulum. *J. Cell Biol.* **182,** 685–701 (2008).

50. Mizushima, N. Autophagy: Process and function. *Genes and Development* **21,** 2861–2873 (2007).

51. Klionsky, D. J. *et al.* In the beginning there was babble... *Autophagy* **8,** 1165–1167 (2012).

52. Hamasaki, M. *et al*. Up-to-date membrane biogenesis in the autophagosome formation. *Current Opinion in Cell Biology* **25,** 455–460 (2013).

53. Russell, R. C. *et al.* ULK1 induces autophagy by phosphorylating Beclin-1 and activating VPS34 lipid kinase. *Nat. Cell Biol.* **15,** 741–50 (2013).

54. Wirth, M. *et al*. Autophagosome formation-The role of ULK1 and Beclin1-PI3KC3

complexes in setting the stage. *Seminars in Cancer Biology* **23,** 301–309 (2013).

55. Kim, J. *et al.* Differential regulation of distinct Vps34 complexes by AMPK in nutrient stress and autophagy. *Cell* **152,** 290–303 (2013).

56. Rubinsztein, D. C. *et al*. Autophagy and aging. *Cell* **146,** 682–695 (2011).

57. Lipinski, M. M. *et al.* Genome-wide analysis reveals mechanisms modulating autophagy in normal brain aging and in Alzheimer's disease. *Pnas* **107,** 14164–14169 (2010).

58. Zhang, C. & Cuervo, A. M. Restoration of chaperone-mediated autophagy in aging liver improves cellular maintenance and hepatic function. *Nat. Med.* **14,** 959–65 (2008).

59. Meléndez, A. *et al.* Autophagy genes are essential for dauer development and life-span extension in C. elegans. *Science* **301,** 1387–91 (2003).

60. Colman, R. J. *et al.* Caloric restriction delays disease onset and mortality in rhesus monkeys. *Science* **325,** 201–204 (2009).

61. Kenyon, C. J. The genetics of ageing. *Nature* **464,** 504–512 (2010).

62. Harrison, D. E. *et al.* Rapamycin fed late in life extends lifespan in genetically heterogeneous mice. *Nature* **460,** 392–395 (2009).

63. Ravikumar, B. *et al.* Regulation of mammalian autophagy in physiology and pathophysiology. *Physiol Rev* **90,** 1383–1435 (2010).

64. Vijg, J. & Campisi, J. Puzzles, promises and a cure for ageing. *Nature* **454,** 1065–1071 (2008).

65. Wu, J. J. *et al.* Mitochondrial dysfunction and oxidative stress mediate the

physiological impairment induced by the disruption of autophagy. *Aging (Albany. NY).* **1,** 425–437 (2009).

66. Sheng, R. *et al.* Autophagy activation is associated with neuroprotection in a rat model of focal cerebral ischemic preconditioning. *Autophagy* **6,** 482–94 (2010).

67. Le Bourg, É. Hormesis, aging and longevity. *Biochimica et Biophysica Acta - General Subjects* **1790,** 1030–1039 (2009).

68. Chen, C. *et al*. mTOR regulation and therapeutic rejuvenation of aging hematopoietic stem cells. *Sci. Signal.* **2,** ra75 (2009).

69. Castilho, R. M. *et al*. mTOR Mediates Wnt-Induced Epidermal Stem Cell Exhaustion and Aging. *Cell Stem Cell* **5,** 279–289 (2009).

70. Levine, B. & Kroemer, G. Autophagy in the Pathogenesis of Disease. *Cell* **132,** 27–42 (2008).

71. Levine, B. *et al*. Autophagy in immunity and inflammation. *Nature* **469,** 323–335 (2011).

72. Saitoh, T. & Akira, S. Regulation of innate immune responses by autophagy-related proteins. *J. Cell Biol.* **189,** 925–35 (2010).

73. Witte, A. V. *et al*. Caloric restriction improves memory in elderly humans. *Proc. Natl. Acad. Sci. U. S. A.* **106,** 1255–60 (2009).

74. Mattson, M. P. & Wan, R. Beneficial effects of intermittent fasting and caloric restriction on the cardiovascular and cerebrovascular systems. *Journal of Nutritional Biochemistry* **16,** 129–137 (2005).

75. Gewirtz, D. A. Autophagy and senescence: A partnership in search of definition.

Autophagy **9,** 808–812 (2013).

76. Gerland, L. M. *et al.* Association of increased autophagic inclusions labeled for β-galactosidase with fibroblastic aging. *Exp. Gerontol.* **38,** 887–895 (2003).

77. Young, A. R. J. *et al.* Autophagy mediates the mitotic senescence transition. *Genes Dev.* **23,** 798–803 (2009).

78. Kang, H. T. *et al*. Autophagy impairment induces premature senescence in primary human fibroblasts. *PLoS One* **6,** (2011).

79. Kang, C. & Elledge, S. J. How autophagy both activates and inhibits cellular senescence. *Autophagy* **12,** 898–899 (2016).

80. Kang, C. *et al.* The DNA damage response induces inflammation and senescence by inhibiting autophagy of GATA4. *Science* **349,** aaa5612 (2015).

81. Levine, B. & Abrams, J. p53: The Janus of autophagy? *Nat. Cell Biol.* **10,** 637–9 (2008).

82. Kuma, A. *et al.* The role of autophagy during the early neonatal starvation period. *Nature* **432,** 1032–1036 (2004).

83. Yan, L. *et al.* Autophagy in chronically ischemic myocardium. *Proc. Natl. Acad. Sci. U. S. A.* **102,** 13807–13812 (2005).

84. Kondo, Y. *et al*. The role of autophagy in cancer development and response to therapy. *Nat. Rev. Cancer* **5,** 726–734 (2005).

85. Fougeray, S. & Pallet, N. Mechanisms and biological functions of autophagy in diseased and ageing kidneys. *Nat. Rev. Nephrol.* **11,** 34–45 (2014).

86. Byrne, C. J. *et al.* Ischemic conditioning protects the uremic heart in a rodent model of myocardial infarction. *Circulation* **125,** 1256–1265 (2012).

87. Liu, C. S. *et al*. H. Biomarkers of DNA damage in patients with end-stage renal disease: mitochondrial DNA mutation in hair follicles. *Nephrol. Dial. Transplant* **16,** 561–565 (2001).

88. Stenvinkel, P. & Alvestrand, A. Inflammation in end-stage renal disease: Sources, consequences, and therapy. *Seminars in Dialysis* **15,** 329–337 (2002).

89. Chen, W. T. *et al.* Impaired leukocytes autophagy in chronic kidney disease patients. *CardioRenal Med.* **3,** 254–264 (2013).

90. Siedlecki, A *et al*. J. Uremic cardiac hypertrophy is reversed by rapamycin but not by lowering of blood pressure. *Kidney Int.* **75,** 800–808 (2009).

91. Odr, M. A. R. *et al*. Replicative senescence in patients with chronic kidney failure. *Kidney Int.* **68,** 11–15 (2005).

92. Tsirpanlis, G. *et al.* Telomerase activity is decreased in peripheral blood mononuclear cells of hemodialysis patients. *Am. J. Nephrol.* **26,** 91–96 (2006).

93. Bansal, N. *et al.* Association between kidney function and telomere length: The heart and soul study. *Am. J. Nephrol.* **36,** 405–411 (2012).

94. Adijiang, A. *et al*. Indoxyl sulfate, a uremic toxin, promotes cell senescence in aorta of hypertensive rats. *Biochem. Biophys. Res. Commun.* **399,** 637–641 (2010).

95. Muteliefu, G. *et al.* Indoxyl sulfate promotes vascular smooth muscle cell senescence with upregulation of p53, p21, and prelamin A through oxidative stress. *AJP Cell Physiol.* **303,** C126–C134 (2012).

96. Carracedo, J. *et al.* Carbamylated low-density lipoprotein induces oxidative stress and accelerated senescence in human endothelial progenitor cells. *FASEB J.* **25,** 1314–22 (2011).

97. Klinkhammer, B. M. *et al.* Mesenchymal stem cells from rats with chronic kidney disease exhibit premature senescence and loss of regenerative potential. *PLoS One* **9,** (2014).

98. Hansen, T. E. & Johansen, T. Following autophagy step by step. *BMC Biol.* **9,** 39 (2011).

99. Mizushima, N. *et al.* Methods in Mammalian Autophagy Research. *Cell* **140,** 313–326 (2010).

100. Klionsky, DJ, et al. Guidelines for the use and interpretation of assays for monitoring autophagy. *Autophagy* **8,** 445–544 (2012).

101. Mizushima, N. & Yoshimori, T. How to interpret LC3 immunoblotting. *Autophagy* **3,** 542–545 (2007).

102. Kabeya, Y. *et al.* Erratum: LC3, a mammalian homolog of yeast Apg8p, is localized in autophagosome membranes after processing (EMBO Journal (2000) 19 (5720-5728)). *EMBO Journal* **22,** 4577 (2003).

103. Ni, H. M. *et al.* Dissecting the dynamic turnover of GFP-LC3 in the autolysosome. *Autophagy* **7,** 188–204 (2011).

104. Bjørkøy, G. *et al.* p62/SQSTM1 forms protein aggregates degraded by autophagy and has a protective effect on huntingtin-induced cell death. *J. Cell Biol.* **171,** 603–614 (2005).

105. Wang, Q. J. *et al.* Induction of autophagy in axonal dystrophy and degeneration. *J. Neurosci.* **26,** 8057–8068 (2006).

106. Nakaso, K. *et al.* Transcriptional activation of p62/A170/ZIP during the formation of the aggregates: Possible mechanisms and the role in Lewy body formation in

Parkinson's disease. *Brain Res.* **1012,** 42–51 (2004).

107. Ropolo, A. *et al.* The pancreatitis-induced vacuole membrane protein 1 triggers autophagy in mammalian cells. *J. Biol. Chem.* **282,** 37124–37133 (2007).

108. Moussay, E. *et al.* The acquisition of resistance to TNFα in breast cancer cells is associated with constitutive activation of autophagy as revealed by a transcriptome analysis using a custom microarray. *Autophagy* **7,** 760–770 (2011).

109. Morchang, A. *et al.* Cell death gene expression profile: Role of RIPK2 in dengue virus-mediated apoptosis. *Virus Res.* **156,** 25–34 (2011).

110. Eskelinen, E. L. *et al*. Seeing is believing: The impact of electron microscopy on autophagy research. *Autophagy* **7,** 935–956 (2011).

111. Mizushima, N. *et al*. In vivo analysis of autophagy in response to nutrient starvation using transgenic mice expressing a fluorescent autophagosome marker. *Mol. Biol. Cell* **15,** 1101–1111 (2004).

112. Bugaut, H. *et al.* Bleomycin Exerts Ambivalent Antitumor Immune Effect by Triggering Both Immunogenic Cell Death and Proliferation of Regulatory T Cells. *PLoS One* **8,** (2013).

113. Feng, B. *et al.* Uraemic serum induces dysfunction of vascular endothelial cells: role of ubiquitin-proteasome pathway. *Exp. Physiol.* **96,** 801–15 (2011).

114. Shimizu, H. *et al.* Indoxyl sulfate downregulates renal expression of Klotho through production of ROS and activation of nuclear factor-κB. *Am. J. Nephrol.* **33,** 319–324 (2011).

115. Yokozawa, T. *et al*. Animal model of adenine-induced chronic renal failure in rats. *Nephron* **44,** 230–234 (1986).

116. Yokozawa, T. *et al*. Metabolic effects of dietary purine in rats. *J. Nutr. Sci. Vitaminol. (Tokyo).* **28,** 519–526 (1982).

117. Garrido, P. *et al.* Characterization of a rat model of moderate chronic renal failure--focus on hematological, biochemical, and cardio-renal profiles. *Ren. Fail.* **31,** 833–842 (2009).

118. Anversa, P. *et al*. Myocyte cell loss and myocyte hypertrophy in the aging rat heart. *J. Am. Coll. Cardiol.* **8,** 1441–1448 (1986).

119. North, B. J. & Sinclair, D. A. The intersection between aging and cardiovascular disease. *Circulation Research* **110,** 1097–1108 (2012).

120. Herzog, C. A. *et al.* Cardiovascular disease in chronic kidney disease. A clinical update from Kidney Disease: Improving Global Outcomes (KDIGO). *Kidney Int* **80,** 572–586 (2011).

121. Moody, W. E. *et al*. Arterial disease in chronic kidney disease. *Heart* **99,** 365–72 (2013).

122. Mitsnefes, M. M. Cardiovascular disease in children with chronic kidney disease. *J. Am. Soc. Nephrol.* **23,** 578–85 (2012).

123. Linton, P. J. *et al*. This old heart: Cardiac aging and autophagy. *Journal of Molecular and Cellular Cardiology* **83,** 44–54 (2015).

124. De Meyer, G. R. Y. *et al*. Role of autophagy in heart failure associated with aging. *Heart Fail. Rev.* **15,** 423–30 (2010).

125. Strait, J. B. & Lakatta, E. G. Aging-Associated Cardiovascular Changes and Their Relationship to Heart Failure. *Heart Failure Clinics* **8,** 143–164 (2012).

126. Kuma, A. & Mizushima, N. Chromosomal mapping of the GFP-LC3 transgene in GFP-LC3 mice. *Autophagy* **4,** 61–62 (2008).

127. Yang, Y.P. *et al.* Application and interpretation of current autophagy inhibitors and activators. *Acta Pharmacol. Sin.* **345,** 625–635 (2013).

128. Wang, L. *et al.* Decreased autophagy: a major factor for cardiomyocyte death induced by beta1-adrenoceptor autoantibodies. *Cell Death Dis.* **6,** e1862 (2015).

129. Weichhart, T. *et al*. Regulation of innate immune cell function by mTOR. *Nat. Rev. Immunol.* **15,** 599–614 (2015).

130. Gustafsson, A. B. & Gottlieb, R. A. Autophagy in ischemic heart disease. *Circ. Res.* **104,** 150–8 (2009).

131. Meijers, B. K. I. & Evenepoel, P. The gut-kidney axis: Indoxyl sulfate, p-cresyl sulfate and CKD progression. *Nephrol. Dial. Transplant.* **26,** 759–761 (2011).

132. Ramírez-Peinado, S. *et al.* Glucose-starved cells do not engage in prosurvival autophagy. *J. Biol. Chem.* **288,** 30387–30398 (2013).

133. Moruno-Manchón, J. F. *et al*. Glucose induces autophagy under starvation conditions by a p38 MAPK-dependent pathway. *Biochem. J.* **506,** 497–506 (2012).

134. Meijers, B. K. I. *et al.* p-cresyl sulfate and indoxyl sulfate in hemodialysis patients. *Clin. J. Am. Soc. Nephrol.* **4,** 1932–1938 (2009).

135. Jiang, Q. *et al.* Heat shock protein 90-mediated inactivation of nuclear factor-κB switches autophagy to apoptosis through becn1 transcriptional inhibition in selenite-induced NB4 cells. *Mol. Biol. Cell* **22,** 1167–1180 (2011).

136. Döring, Y. *et al*. The CXCL12/CXCR4 chemokine ligand/receptor axis in cardiovascular

disease. *Front. Physiol.* **5 JUN,** (2014).

137. Liehn, E. A. *et al.* Double-edged role of the CXCL12/CXCR4 axis in experimental myocardial infarction. *J. Am. Coll. Cardiol.* **58,** 2415–2423 (2011).

138. Alhaj, E. *et al.* Uremic cardiomyopathy: An underdiagnosed disease. *Congestive Heart Failure* **19,** (2013).

139. Wu, H. *et al.* The BCL2L1 and PGAM5 axis defines hypoxia-induced receptor-mediated mitophagy. *Autophagy* **10,** 1712–1725 (2014).

140. Goldman, R. D. *et al*. Nuclear lamins: Building blocks of nuclear architecture. *Genes and Development* **16,** 533–547 (2002).

141. De Sandre-Giovannoli, A. *et al.* Lamin a truncation in Hutchinson-Gilford progeria. *Science* **300,** 2055 (2003).

142. Baker, D. J. *et al.* BubR1 insufficiency causes early onset of aging-associated phenotypes and infertility in mice. *Nat. Genet.* **36,** 744–9 (2004).

143. Maroz, N. & Simman, R. Wound Healing in Patients With Impaired Kidney Function. *J. Am. Coll. Clin. Wound Spec.* **5,** 2–7 (2013).

144. Nacken, W. *et al.* S100A9/S100A8: Myeloid representatives of the S100 protein family as prominent players in innate immunity. *Microsc. Res. Tech.* **60,** 569–580 (2003).

145. McCormick, M. M. *et al.* S100A8 and S100A9 in Human Arterial Wall. *J. Biol. Chem.* **280,** 41521–41529 (2005).

146. Hanssen, N. M. *et al.* Higher levels of advanced glycation endproducts in human carotid atherosclerotic plaques are associated with a rupture-prone phenotype. *Eur*

Hear. J (2013). doi:10.1093/eurheartj/eht402

147. Healy, A. M. *et al.* Platelet expression profiling and clinical validation of myeloid-related protein-14 as a novel determinant of cardiovascular events. *Circulation* **113,** 2278–2284 (2006).

148. Altwegg, L. A. *et al.* Myeloid-related protein 8/14 complex is released by monocytes and granulocytes at the site of coronary occlusion: A novel, early, and sensitive marker of acute coronary syndromes. *Eur. Heart J.* **28,** 941–948 (2007).

149. Croce, K. *et al.* Myeloid-related protein-8/14 is critical for the biological response to vascular injury. *Circulation* **120,** 427–436 (2009).

150. Mizushima, N. & Kuma, A. Autophagosomes in GFP-LC3 transgenic mice. *Methods Mol. Biol.* **445,** 119–124 (2008).

151. Sengstock, D.M. *et al.* Homeostatic intracellular repair response (HIR2) is increased in older adults and is upregulated by ischemia. *J. Am. Geriatr. Soc.* **62,** S108 (2014).

152. Dou, L. *et al.* The uremic solute indoxyl sulfate induces oxidative stress in endothelial cells. *J. Thromb. Haemost.* **5,** 1302–1308 (2007).

153. Filomeni, G. *et al*. Oxidative stress and autophagy: the clash between damage and metabolic needs. *Cell Death Differ.* **22,** 377–388 (2015).

154. Scherz-Shouval, R. *et al.* Reactive oxygen species are essential for autophagy and specifically regulate the activity of Atg4. *EMBO J.* **26,** 1749–60 (2007).

155. Taneike, M. *et al.* Inhibition of autophagy in the heart induces age-related cardiomyopathy. *Autophagy* **6,** 600–606 (2010).

156. Rajawat, Y. S. *et al*. Aging: Central role for autophagy and the lysosomal degradative

system. *Ageing Research Reviews* **8,** 199–213 (2009).

157. Wohlgemuth, S. E. *et al.* Autophagy in the heart and liver during normal aging and calorie restriction. *Rejuvenation Res.* **10,** 281–92 (2007).

158. Boyle, A. J. *et al.* Cardiomyopathy of aging in the mammalian heart is characterized by myocardial hypertrophy, fibrosis and a predisposition towards cardiomyocyte apoptosis and autophagy. *Exp. Gerontol.* **46,** 549–559 (2011).

159. Dirks-Naylor, A. J. The role of autophagy in doxorubicin-induced cardiotoxicity. *Life Sci.* **93,** 913–916 (2013).